Scientific Reports

https://doi.org/10.1038/s41598-026-39600-6

Article in Press

Mechanical annealing in a soft granular layer under cyclic shear at varying frequencies

Received: 28 November 2024

Accepted: 6 February 2026

Published online: 14 February 2026

Cite this article as: Tapia-Ignacio C., Fossion R.Y.M. & López-González F. Mechanical annealing in a soft granular layer under cyclic shear at varying frequencies. *Sci Rep* (2026). https://doi.org/10.1038/s41598-026-39600-6

Cecilio Tapia-Ignacio, Ruben Yvan Maarten Fossion & Francisco López-González

Mechanical annealing in a soft granular layer under cyclic shear at varying frequencies

Cecilio Tapia-Ignacio[1,2], Ruben Yvan Maarten Fossion[2,3], and Francisco López-González[1,4,*]

[1]Autonomous University of the State of Hidalgo, Institute of Basic Sciences and Engineering, Pachuca, Hidalgo 42184, Mexico
[2]National Autonomous University of Mexico (UNAM), Institute of Nuclear Sciences, Mexico City 04510, Mexico
[3]National Autonomous University of Mexico (UNAM), Center for Complexity Sciences (C3), Mexico City 04510, Mexico
[4]National Polytechnic Institute (IPN), Higher School of Mechanical and Electrical Engineering, Zacatenco Unit (ESIME), Mexico City 07700, Mexico
[*]email: francisco_lopez@uaeh.edu.mx

ABSTRACT

In the present work, we present a two-dimensional soft sphere granular system, with inclination, that models the transition from an amorphous solid to the crystalline phase by shear cycles induced by cyclic deformations of the boundary. To simulate an effective temperature, the system is subjected to vibration. Under these conditions, the system exhibits a controlled transition to hexagonal order, where the crystallization rate and extent depend critically on the shear frequency. The study focuses on the analysis of the effect of the shear frequency in phase change, and introduces a dimensionless shear frequency $\tilde{f} = f_s \tau_r$, where $\tau_r = \sqrt{m/k}$ is the intrinsic relaxation timescale of the particles, to identify the regimes in which mechanical annealing is effective. The soft granular particles used are polyacrylamide hydrogel spheres, with an estimated Young's modulus of the order of 10^4 Pa, consistent with previous measurements for single-network polyacrylamide gels. Hexagonal order is measured in terms of the sixth-bond orientational order parameter ψ_6'. By following the temporal evolution of this parameter, we find that low shear frequencies on the order of 10^{-3} Hz (i.e., $\tilde{f} \ll 1$) favor the growth of hexagonal grains, while higher frequencies tend to reduce hexagonal order, leading to an unstable structure. Additionally, we characterize particle dynamics through autocorrelation measurements in the time series of ψ_6' using Fourier spectral analysis (FA). For all cases with non-zero shear frequency, the power spectra follow a power law, $P(f) \propto 1/f^{\beta}$ with $\beta > 1$, indicating non-stationarity. In contrast, for the static (0 Hz in shear frequency) case, the power spectrum is flat ($\beta \approx 0.04$), suggesting stationary white noise behavior in the time series.

Introduction

Solid-to-solid phase transitions induced through mechanical perturbations are an interesting subject of study[1–10] because they provide an alternative method to traditional thermal treatments. Recent theoretical advances have established non-equilibrium thermodynamic frameworks for understanding these mechano-structural transitions[11], while new experimental techniques enable precise observation of particle-scale reorganization[12,13].

Among the different types of mechanical stresses, shear force receives special attention as it plays a crucial role in various applications, including designing structures, understanding fluid flow, and analyzing the behavior of materials under different mechanical conditions. In particular, oscillatory shear has emerged as a powerful tool for controlling material microstructure, with frequency-dependent effects observed across colloidal, granular, and polymeric systems[5,6]. The measurement and analysis of shear stress are essential for predicting and preventing material failure and understanding the deformation characteristics of solids and fluids. In some studies, shear forces are used to disarrange hard-sphere systems[8]. However, under certain conditions they can also be used to improve crystalline order[1] even in hard cube systems[2,9]. For example, in Ref.[6] a shear stress induced by mechanical oscillations around 70 Hz, applied in the stagnant liquid of a colloidal suspension, increased the nucleation rate in a hard-sphere colloidal glass. In colloidal gels, shear frequencies also play an important role to reach the point at which the observation of crystallization, provoking yielding, occurs. In Ref.[10] it is reported that as the frequency of oscillatory shearing increased (at 1, 10, and 70 Hz) in colloidal gels, the strain amplitude necessary for yielding or crystallization decreased. This aligns with contemporary understanding of yielding transitions in soft glassy materials, where frequency-amplitude coupling governs the onset of structural reorganization[14–16].

In granular systems, mechanical annealing can be achieved solely through the application of vibrations[7,17]. However, this

process can be optimized by combining cyclic shear forces with vibration[1,2,18]. Recent work has revealed universal scaling laws in the vicinity of the jamming transition of sheared granular materials[19], while the synergistic effects of shear-vibration coupling remain an active area of investigation. Depending on particle shape, different values of shear strain and frequency to anneal a granular ensemble are reported. For example, in a hard cube system, a high shear strain at 0.05 Hz tends to favor crystallization[2], whereas in a hard sphere system, a small shear strain at 0.10 Hz reduces the appearance of shear banding and promotes crystallization[1].

Recent works have shown that ordering dynamics in granular media are strongly dependent on boundary conditions and system geometry. For instance, crystallization in vibrated granular spheres may occur heterogeneously at the walls[20], while the use of cyclic shear significantly accelerates and stabilizes the formation of ordered phases[3,7,21]. The combination of vibration and shear has been shown to be more efficient than vibration alone in inducing ordering transitions, with the onset of crystallization governed by a delicate balance between amplitude, frequency, and particle shape[22,23].

These behaviors extend beyond rigid particles. In soft granular systems such as those composed of hydrogel spheres, the mechanical response is governed not only by contact geometry but also by the viscoelastic nature of the particles[24]. Recent studies show that properties such as particle softness, surface fuzziness, and relaxation timescales play an important role in the rheological response and ordering dynamics under stress[25,26]. The macroscopic behavior of these systems emerges from microscale interactions modulated by stiffness, surface chemistry, and compressibility[27]. To bridge microscopic and macroscopic behavior in granular and colloidal systems, novel approaches have been developed using graph-theoretical descriptors and dimensionless parameters that capture structural fluctuations across multiple scales[28]. These tools complement traditional order parameters and allow for the detection of subtle phase transitions or dynamical regimes not easily observable via conventional metrics. Beyond phenomenological observations, recent studies have emphasized the importance of particle-scale rearrangements and collective dynamics in mechanically driven disordered systems. In particular, network-based and trajectory-resolved approaches have provided new insight into the transition from quasi-static to dynamically evolving regimes in granular assemblies subjected to slow compression or shear. These works demonstrate that even under low driving rates, subtle changes in contact networks and force chains can signal the onset of irreversible rearrangements and structural reorganization[29,30]. Related concepts have also been explored in amorphous solids and soft glassy materials, where oscillatory or steady shear can encode memory effects and induce history-dependent responses[31]. In this context, shear-driven reorganization has been shown to give rise to non-trivial dynamical transitions, characterized by changes in particle trajectories and collective yielding behavior. These findings highlight that mechanically induced ordering or disordering cannot be understood solely in terms of instantaneous strain, but rather emerges from the interplay between driving protocols and internal relaxation processes. At higher densities, the connection between mechanical annealing and the jamming transition becomes particularly relevant. Previous studies have shown that macroscopic yielding in jammed solids is accompanied by abrupt, nonequilibrium changes in particle trajectories, suggesting a transition-like behavior driven by external forcing rather than thermal fluctuations[32]. While our experiments remain in a low-frequency, quasi-static regime, these results provide a broader framework for interpreting shear-induced structural crossovers in terms of proximity to jamming and relaxation-limited dynamics.

Consequently, there are not a general theory describing an operational range, in terms of amplitude and frequency, in which cyclic shear forces influences the phase transitions from amorphous to crystalline or between crystalline phases when different particle shapes are chosen. Recent attempts to develop such frameworks include mesoscale elastoplastic models[33] and jamming phase diagrams[34], though significant challenges remain in unifying observations across different systems. In this work, we envisage to contribute to the state-of-art of mechanical annealings for nearly-hard systems by considering a two-dimensional soft sphere granular sample, composed of millimetric hydrogel balls. The system is enclosed by a deformable rectangular boundary through which periodic one-dimensional shear is provided. Mechanical vibrations are applied separately using a speaker to fluidize the spheres. A slight inclination of the system provides a component of gravity used as attractive force in order to gather the particles at the bottom of the boundary. We include two supplementary videos showing the experimental dynamics. Supplementary Video S1 presents the behavior of the granular system under vibration without shear, serving as a reference for particle motion and ordering. Supplementary Video S2 shows the system under cyclic shear at a frequency of 0.1 Hz with maximum angular deformation of 0.41 radians, making evident the shear-induced deformation of the boundary. We foresee that our study can model mechanical annealings of concentrated suspensions of nearly hard colloidal spheres[35] as studied in[5,6] since both systems exhibit frequency-dependent ordering behavior under oscillatory driving. In particular, in our system, mechanical vibration generates an effective temperature that drives structural rearrangements. Due to the two-dimensional nature of the system, the movement of all particles was monitored, and the order parameters were calculated individually for each particle. We investigated the dynamic progression of the hexagonal order within the system, starting from an almost amorphous state and culminating in a crystalline state. The analysis was carried out at various maximum deformation shear frequency and amplitude values. The hexagonal order is measured by means of the sixth-bond orientational order parameter ψ_6', which has proven to be effective in identifying the HCP crystalline phase[5,6,36,37].

To complement the study, we use time-series analysis techniques to characterize the system's dynamics directly, quantifying

the strength of correlations in the time series of the sixth-bond orientational order parameter ψ_6' through Fourier spectral analysis. We do not delve into the origins of this behavior here, some of which we have explored in previous work. Specifically, we have previously applied Fourier spectral analysis techniques to magnetic particles driven by a time-dependent magnetic field in a two-dimensional medium and to ellipsoidal particles moving over magnetic particles. In these cases, we found that, under certain conditions, the power spectra follow a power law, $P(f) \propto 1/f^{\beta}$ with $\beta \approx 2$, indicating scale invariance and Brownian-like motion in the respective time series[38–40]. In the present system, we show that the system exhibits non-stationary behavior, when the shear frequencies are different from zero.

The paper is organized as follows. First, we explore the temporal evolution of hexagonal ordering in the soft-sphere granular system subjected to mechanical annealing induced by cyclic shear deformations. To this end, we first analyze the system's dynamics in the absence of shear forces, studying the effects of vibrations alone on the ordering process. Then, we investigate the behavior of the system under varying shear frequencies, examining how cyclic deformations influence the development of hexagonal order. Next, we delve into the time-series analysis techniques used to characterize the non-stationary behavior of the system through Fourier analysis, showing that the power spectra follow a power law, which confirms the non-stationary dynamics of the system. Then we summarize the key findings, discussing the varying degrees of order observed depending on shear frequency and suggesting directions for future research, such as expanding the shear frequency range and investigating the role of particle shape and boundary conditions in the ordering dynamics. Finally, we describe the experimental setup and define the orientational order parameter used in our study to quantify the degree of crystalline ordering.

Results and discussion

Vibrated reference system without shear. We studied the temporal evolution of the hexagonal order by tracking the average value of the sixth bond-orientational order parameter of each sphere at time t. Fig. 1 shows the temporal evolution of hexagonal ordering under vibration in the absence of shear. In Fig. 1-(a), the graph of $< \psi_6' >$ versus time is presented, highlighting an exponential fit (red). As it is seen, hexagonal order presents a relaxation behavior converging in values around 0.76 ± 0.009 after 150 seconds. This relaxation dynamics was fitted using an exponential function, obtaining a relaxation time with a value of 58.14 seconds. This indicates that vibration, along with the inclination, significantly influences the hexagonal ordering without achieving a fully hexagonal arrangement of the entire ensemble. Fig. 1-(b) offers a visual representation through color maps of the sixth bond-orientational order parameter, where the color scale indicates the specific value of ψ_6' for each particle. In these maps, the bottom of the container is positioned to the left. The images correspond to a representative experiment selected from a group of five repeated tests showing similar behavior. While variability is expected due to the stochastic nature of vibrational dynamics, the qualitative trends reported here were consistently observed.

As we can observe, distinct hexagonal clusters appear at the beginning of the experiment, showing a slight tendency to nucleate at the walls. During the first 5 seconds, it was noted that the clusters grow through coalescence, with a large cluster initially forming near the right-hand wall of the container. However, this cluster disintegrates due to gravitational forces. In contrast, a more stable cluster emerges and grows near the lower wall (corresponding to the inclined base), likely due to the combined effects of vibration and gravity. Subsequently, around 50 seconds in, the vibrational dynamics compact the assembly. At 100 seconds, the lower cluster increases in size, and a small central nucleus is observed alongside smaller hexagonal aggregates containing between 2 and 5 particles. By 150 seconds, some of these aggregates are seen to coalesce towards the walls, and, as expected, the cluster with the greatest coalescence is found on the lower wall due to the influence of gravity. Finally, it is observed that this configuration does not present major changes by the end of the experiment, resulting in a mixed configuration with crystalline grains and regions displaying a disordered phase. These visualizations allow for a clearer understanding of the spatial and temporal distribution of hexagonal order in the system. This experiment is used as a reference case to characterize the system's relaxation behavior under vibration alone, and to serve as a baseline for comparison with the experiments conducted under shear. A video of this reference experiment is provided as Supplementary Video S1.

Effect of shear frequency. The first case of shear analyzed and discussed corresponds to a shear frequency of 0.001 Hz. In Fig. 2, the statistical analysis of the sixth bond-orientational order parameter $< \psi_6' >$ is presented. In part (a), the temporal evolution of the hexagonal order is shown in relation to the total duration of the experiment, which spans approximately two shear cycles. As we can see, the curve exhibits a complex oscillatory pattern, oscillating around 0.86, with local maxima around 0.90. Fig. 2-(b) presents the averaged curves of the two shear cycles during the experiment, resulting in the average behavior of $< \psi_6' >$ over an arbitrary shear cycle. The moments of maximum and minimum deformation are marked with dashed vertical lines in red and blue, respectively. A descending trend is observed in the first half of the cycle and an ascending trend in the second half, suggesting that the ordering tendency alternates between moments of maximum deformation. Regarding the descriptive statistics of the values of $< \psi_6' >$, Fig. 2-(c) shows the histogram for the total duration of the experiment. As expected, according to the central limit theorem, the distribution of means follows a Gaussian behavior, with a mean of 0.87 and a standard deviation of 0.03. This indicates low volatility in the values of $< \psi_6' >$ and high stability in the data collection

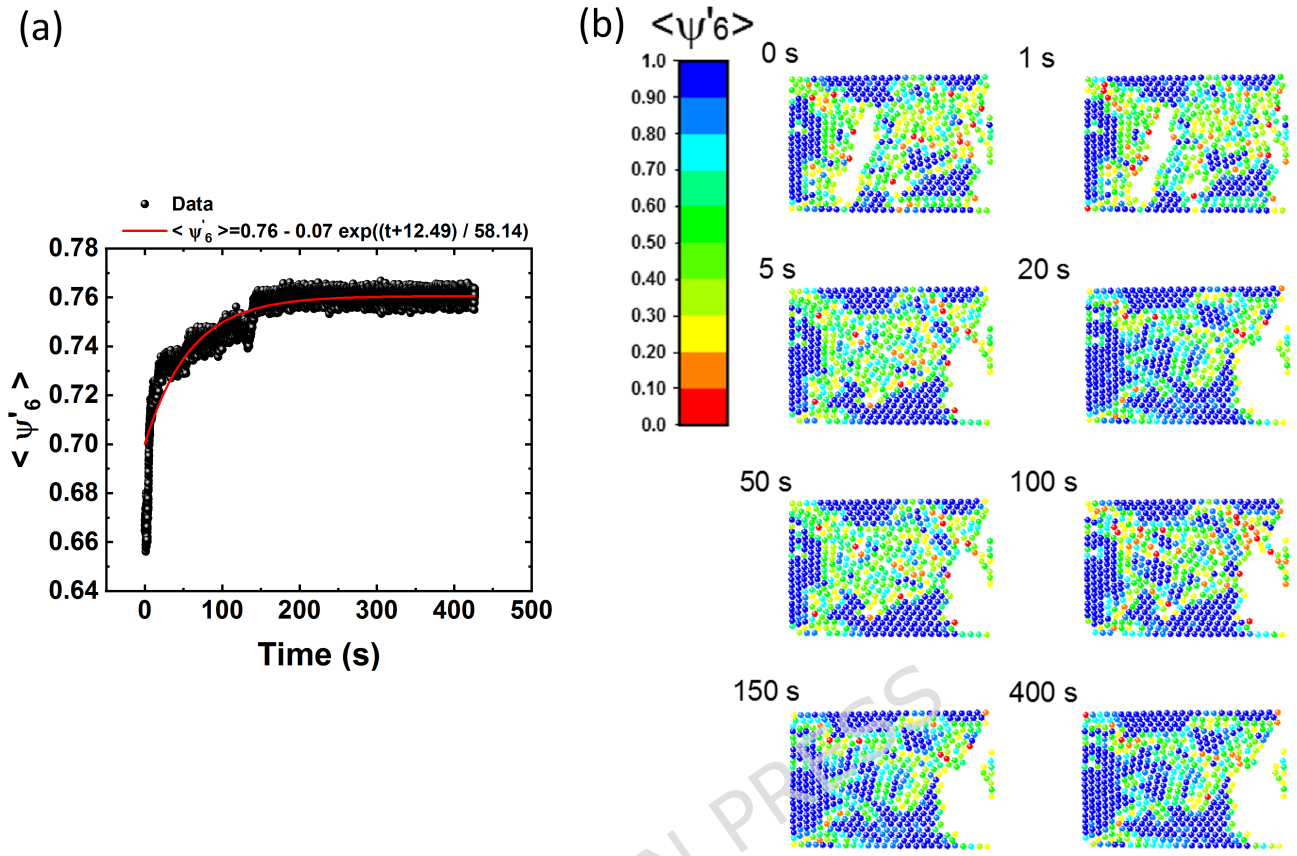

Figure 1. Temporal evolution of hexagonal ordering in the reference experiment with vibration, in the absence of shear. (a) Graph of $\psi_6^{'}$ versus time, showing an exponential fit (red) that describes the growth of orientational order. (b) Color maps of the sixth bond-orientational order parameter, where the color scale indicates the value of $\psi_6^{'}$ for each particle. In these maps, the bottom of the container is oriented to the left. A video of this experiment is available as Supplementary Video S1.

procedure. Finally, in Fig. 2-(d), the mean values of $< \psi_6^{'} >$ per shear cycle are reported, showing an increase of 0.03 from the initial value to the end of the second cycle.

The experimental case obtained by varying the frequency to 0.002 Hz is analyzed below. Figure 3 shows the global statistics of the sixth bond-orientational order parameter $< \psi_6^{'} >$. In this case, we observe that the trend of the $< \psi_6^{'} > (t)$ curve, shown in Fig. 3-(a), follows a relaxation pattern from the beginning of the experiment until approximately 1300 seconds, oscillating around 0.86 and reaching values close to 0.9 by the end of the experiment. To study the trend of hexagonal ordering during a shear cycle, the average curve for the four shear cycles is shown in Fig. 3-(b). The resulting oscillation exhibits three concavities and three convexities, distributed with two concavities and one convexity in the first half of the cycle, and two convexities and one concavity in the second half. The moments of maximum and minimum deformation of the boundary are indicated by red and blue dashed lines, respectively. Alternating hexagonal order maxima and minima can be observed during consecutive moments of maximum deformation, while hexagonal order maxima occur during the minimum deformation stages. The histogram of $< \psi_6^{'} >$ values is shown in Fig. 3-(c), which fits a Gaussian distribution with greater kurtosis than the 0.001 Hz case. The reported mean and standard deviation are 0.86 ± 0.042, indicating a slight decrease in the mean order and a slight increase in the deviation compared to the 0.001 Hz shear case. This suggests that we are dealing with a slightly less stable and, consequently, less ordered process. Finally, Fig. 3-(d) reports the average $< \psi_6^{'} >$ values per shear cycle (SC). We observe a relaxation trend that we fit to an exponential $< \psi_6^{'} >=< \psi_6^{'} >_0 + A_1 \exp(-(SC - SC_0)/\tau)$ with a relaxation value of $\tau = 0.43$ cycles and parameters $< \psi_6^{'} >_0 = 0.87$, $A_1 = -0.09$, and $SC_0 = 0$.

Direct observations from the sample are included. In Fig. 4-(a), the color maps of $< \psi_6^{'} >$ at the initial moments are presented. Meanwhile, in Fig. 4-(b) and Fig. 4-(c), the color maps corresponding to the moments of maximum and minimum deformation in the first and last shear cycles, respectively, are displayed. As we can observe, the sample starts with different hexagonal grains separated by disordered regions and a large void. Within these grains, we identify a central one of large

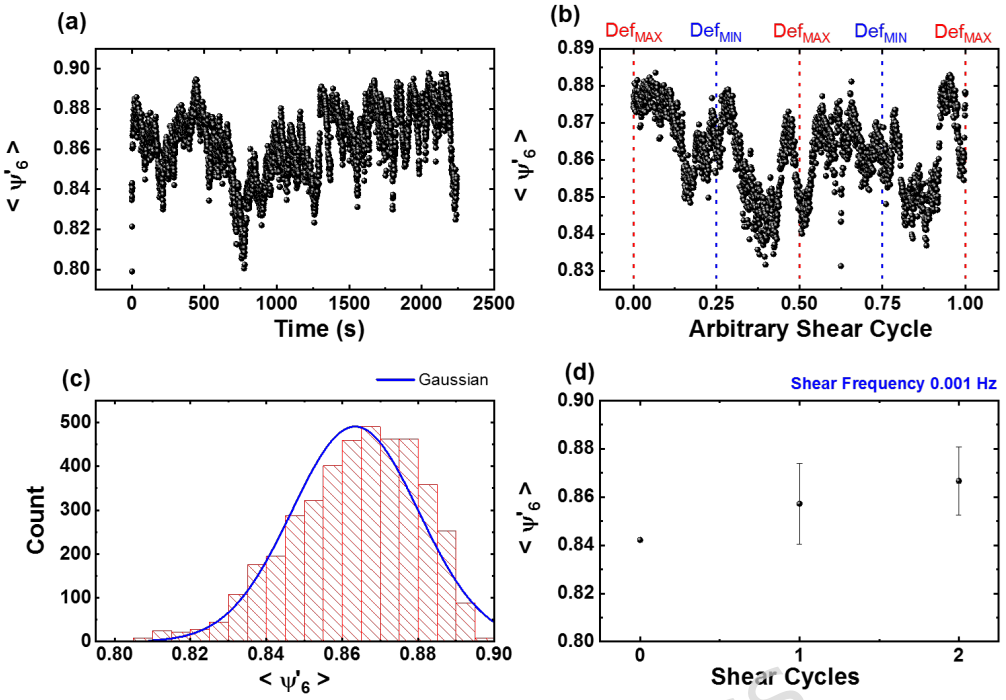

Figure 2. Statistical analysis of the sixth order-bond orientational parameter for cyclic deformations at 0.001 Hz. (a) Plot of the global average $< \psi_6^{'} >$ of the ensemble measured every second throughout the entire duration of the experiment. (b) Average $< \psi_6^{'} >$ curve of the shear cycles. (c) Histogram and normal fit. (d) Average values of $< \psi_6^{'} >$ (and standard deviations) per shear cycle.

size. We can appreciate that from seconds 1 and 2, this grain slightly decreases to fill the void; however, when it separates, a new, smaller void is generated on the upper edge of the grain. Half a second later, the upper grains start disappearing into this void. After this moment and up to 5 seconds, no large voids appear. Instead, approximately five large grains are delineated, isolated by loops that disperse polygonally. These grains are composed of particles with lower hexagonal order, characterized by values of $< \psi_6^{'} >$ ranging between 0.4 and 0.6. At 130 seconds, the first minimum deformation is reached in the boundary. In Fig. 4-(b), we observe that the five grains have coalesced to form two larger grains, along with one significantly smaller grain embedded in a region characterized by poor hexagonal order. A quarter of a cycle later, when the first maximum deformation is reached, we observe that the poorly ordered regions rearrange in the form of loops that act as frontiers of 3 grains, two of which coalesce at the next minimum deformation, improving the hexagonal order. However, there are still disordered polygonal segments that rearrange at the next maximum deformation occurring at 505 seconds. As we can see, once the next minimum deformation is reached, the polygonal regions shift to the sides, promoting the concentration of particles with hexagonal order in the central part. This same dynamics is observed in the last shear cycle, shown in Fig. 4-(c), with the difference that the central grain is larger than at the end of cycle 1. This suggests that the annealing mechanism involves displacing the disordered regions to the sides through deformations, initially concentrating them at points of maximum deformation and then shifting them sideways during stages of minimal deformation. As a result, the disordered regions are gradually reduced with each cycle. The improvement in hexagonal order throughout the entire shearing process is illustrated in Fig. 4-(d), which compares the assembly at the beginning and end of the experiment.

Now, let us analyze the effect of shear at 0.01 Hz. In Fig. 5 the graphs of the temporal evolution of the sixth order-bond orientational parameter $< \psi_6^{'} >$ are displayed for the total experiment duration (Fig. 5-(a)), the hexagonal order behavior per cycle (Fig. 5-(b)), its histogram (Fig. 5-(c)), and the evolution of the average value of $< \psi_6^{'} >$ for each experimental shear cycle (Fig. 5-(d)). As seen in Fig. 5-(a), the increase in frequency generates a higher number of cycles during the experimental time, resulting in a profile shaped like an inverted "L", which can be fitted to an exponential relaxation trend $< \psi_6^{'} >= y_0 + A_1 \exp((-(x-x_0)/\tau)$ with parameters $y_0 = 0.83 \pm 0.002$, $A_1 = -0.21$, $x_0 = -0.069$, and $\tau = 0.39 \pm 0.4$. On the other hand, the average hexagonal order decreases compared to the previous experimental cases, reaching values of 0.848 ± 0.02. Regarding the hexagonal order behavior per cycle, a more defined oscillation than in the previous experimental

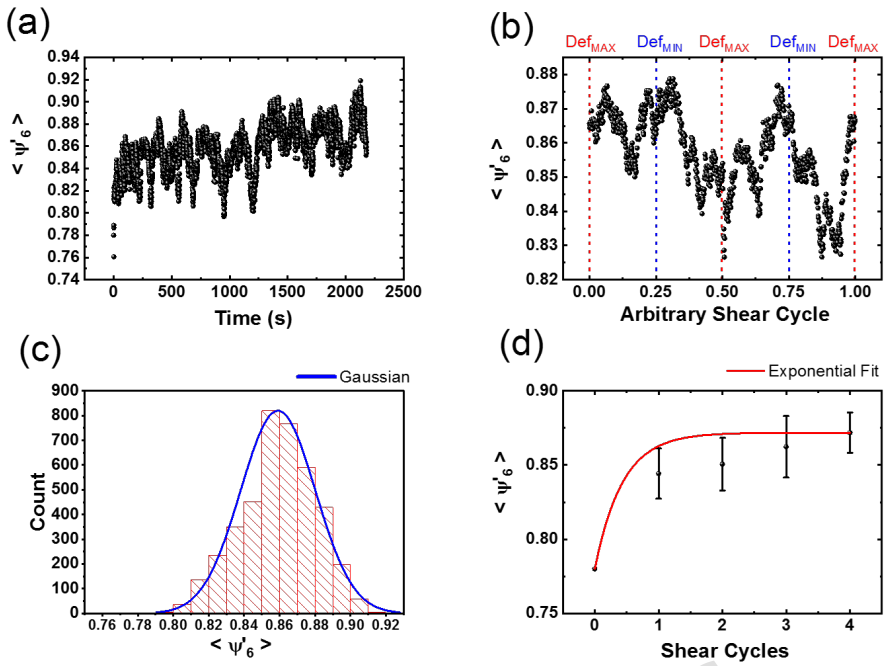

Figure 3. Statistical analysis of the sixth order-bond orientational parameter for cyclic deformations at 0.002 Hz. (a) Plot of the global average $< \psi_6^{'} >$ of the ensemble measured every second throughout the entire duration of the experiment. (b) Average $< \psi_6^{'} >$ curve of the shear cycles. (c) Histogram and normal fit. (d) Average values of $< \psi_6^{'} >$ (and standard deviations) per shear cycle and exponential fit.

cases can be observed, which fits a sinusoidal model. Specifically, we used the model $y = y_0 + a\sin((\pi(x-x_c))/\omega)$ with $y_0 = 0.85 \pm 4.4 \times 10^{-4}$, $a = 0.008 \pm 0.001$, $x_c = 0.06 \pm 0.01$, and $\omega = 0.25 \pm 0.006$. With respect to the process stability, we observe in Fig. 5-(c) a wider Gaussian distribution spanning a broader interval compared to previous experimental cases, indicating increased variability. Finally, concerning the average behavior per cycle, we again observe a relaxation trend in the shape of an inverted "L", which is fitted by the relaxation exponential function $< \psi_6^{'} >= y_0 + A_1 \exp((-(x-x_0))/\tau)$ with parameters $y_0 = 0.848 \pm 0.002$, $A_1 = -0.26$, $x_0 = -0.071$, and $\tau = 0.47 \pm 0.6$.

The highest shear frequency considered was 0.25 Hz. In Fig. 6, statistics of the sixth order-bond orientational $< \psi_6^{'} >$ are shown over the total time of the experiment under four different criteria. In Fig. 6-(a), the graph $< \psi_6^{'} >$ against time is shown over the duration of the experiment. As observed, the high shear frequency quickly drives the system to $< \psi_6^{'} >$ values oscillating around 0.80 with greater dispersion compared to previous experimental cases. Additionally, the absence of the inverted-L relaxation feature seen in series with lower shear frequencies is noted. Averaging the shear cycles and normalizing the domain over a single cycle yields the graph shown in Fig. 6-(b). Similar to the experimental case with a shear frequency of 0.01 Hz, the data exhibit a sinusoidal trend over the cycle, but with a better fit, with maxima near moments of maximum-to-minimum deformation and minima at minimum-to-maximum deformation. Specifically, the fit is given by $y = y_0 + a\sin((x-x_c)/\omega)$ with $y_0 = 0.80 \pm 1 \times 10^{-3}$, $a = 0.015 \pm 0.002$, $x_c = 0.013 \pm 0.02$, and $\omega = 0.26 \pm 0.008$, providing an R^2 value of 0.77. In Fig. 6-(c), the histogram of $< \psi_6^{'} >$ values over the experiment is shown, once again indicating a Gaussian behavior with a mean of 0.8 and a standard deviation of 0.05; reaching the highest standard deviation among the experimental series. This volatility can also be seen in Fig. 6-(d), where the average values and standard deviations per cycle throughout the experiment are plotted. Although variability is maximal relative to previous experimental series, the values display complex oscillatory patterns contained within a range of 0.75 to 0.85. Likewise, the high variability hinders standard function fitting. Nevertheless, a sinusoidal fit is reported, yielding the highest R^2 values found within the set of fitted curves provided by Origin 2018. The fit is given by $y = y_0 + a\sin((x-x_c)/\omega)$ with $y_0 = 0.8 \pm 7.7 \times 10^{-4}$, $a = 0.003 \pm 0.001$, $x_c = 135 \pm 8.5$, and $\omega = 69.3 \pm 8.4$.

With the information obtained from the studied cases, a comparative analysis was conducted. Fig. 7 shows the average value of the orientational order parameter $\langle \psi_6^{'} \rangle$, computed over the entire 30-minute experiment, as a function of the shear frequency

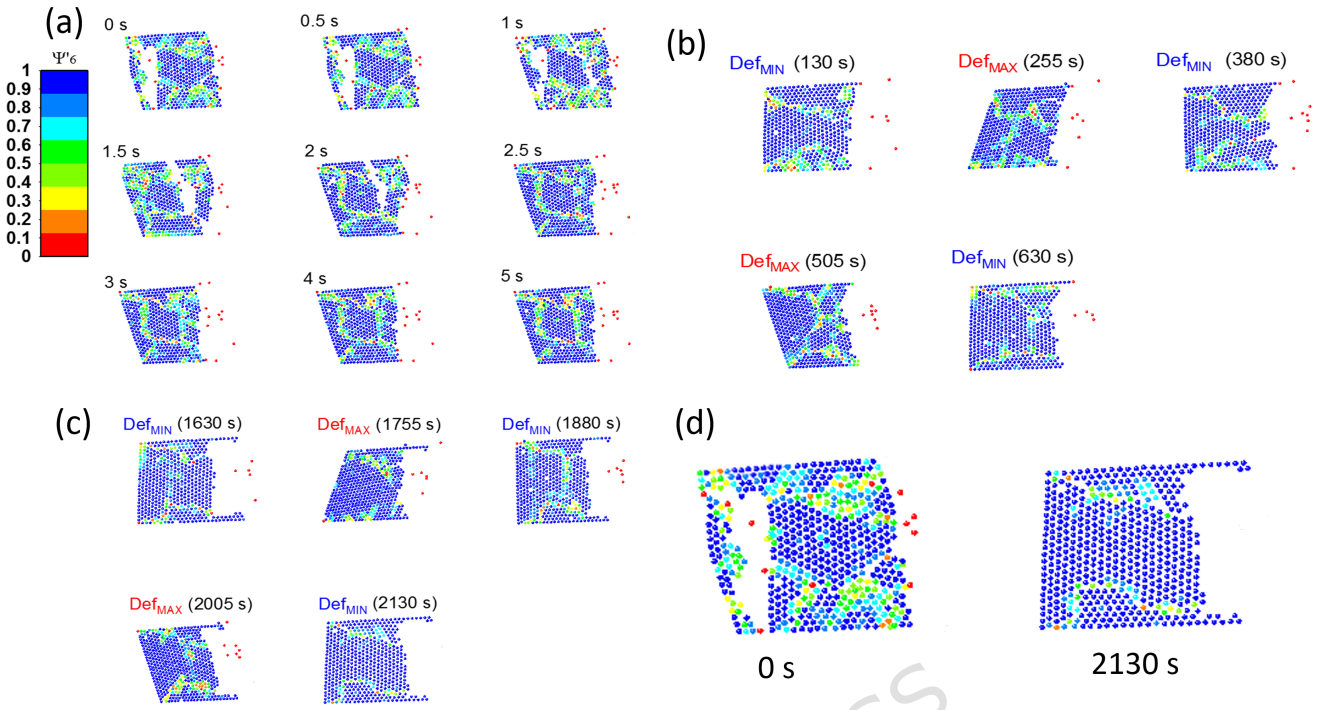

Figure 4. Color maps of the temporal evolution of hexagonal ordering in the experimental case with shear at 0.002 Hz (a) at initial moments and at moments of minimal (DEF_{MIN}) and maximal (DEF_{MAX}) deformation of the boundary for the first (b) and last (c) shear cycles. In these maps, the bottom of the container is positioned to the left. (d) A comparison of the assembly between the beginning and the end of the experiment.

f_s. A clear increase in hexagonal order is observed as the shear frequency decreases. This increase, however, is bounded, with $\langle\psi_6'\rangle$ varying approximately between 0.80 at high shear frequencies and 0.86 in the low-frequency limit. Notably, even at the highest shear frequency explored, the orientational order exceeds the value measured in the vibrated reference system (green dashed line), indicating that cyclic shear within the investigated frequency range systematically enhances hexagonal order. Nevertheless, the system does not reach a fully ordered state, likely due to deformation-induced heterogeneities such as shear band formation. The dependence of $\langle\psi_6'\rangle$ on f_s is well described by an exponential approach to a high-frequency asymptotic value,

$$\langle\psi_6'\rangle(f_s) = \langle\psi_6'\rangle_\infty + (\langle\psi_6'\rangle_0 - \langle\psi_6'\rangle_\infty)\exp(-f_s/f_c), \tag{1}$$

where $\langle\psi_6'\rangle_0$ denotes the low-frequency limit, $\langle\psi_6'\rangle_\infty$ the asymptotic value at high shear frequencies, and f_c a characteristic shear frequency. The fit yields $\langle\psi_6'\rangle_\infty = 0.803 \pm 0.006$, $\langle\psi_6'\rangle_0 = 0.857 \pm 0.009$, and $f_c = 0.082 \pm 0.026$ Hz, with a coefficient of determination $R^2 = 0.95$.

Fourier analysis (FA). The experimental videos analyzed consisted of 1800 frames. Each video is converted to frames with a program called VirtualDub. When opening the video in VirtualDub, we use the interlaced format to a better sharpness for the movement. The video files were taken at 30 fps in AVI interlaced format. From the videos, image sequences were obtained. During the decompression process, we used a filter to separate odd and even frames; thus, we obtained a time resolution of 1/60 s. Using ImageJ and its plugin Mosaic[42], we obtained the trajectories of the particles. These trajectories were then interpreted as time series to obtain the corresponding Fourier power spectra. Examples of times series of the positions in the direction of the sixth bond orientational order parameter ψ_6' of the two-dimensional soft sphere granular system, with inclination, for different values of frequency f, are shown in Fig. 8.

Fourier analysis (FA) is a standard technique widely employed in time-series and signal analysis. It decomposes a time series or signal into a combination of sinusoidal waves, each with a specific frequency f, and amplitude $A(f)$. The Fourier spectrum $P(f)$, gives a representation of such decomposition[43]. It is calculated as the square of the absolute value of the Fourier transform of the time series or signal. In this context, it determines whether correlations are present and their nature[44,45]. When dealing with time series in which fragments of multiple sizes are statistically self-similar to the entire series (fractal time series),

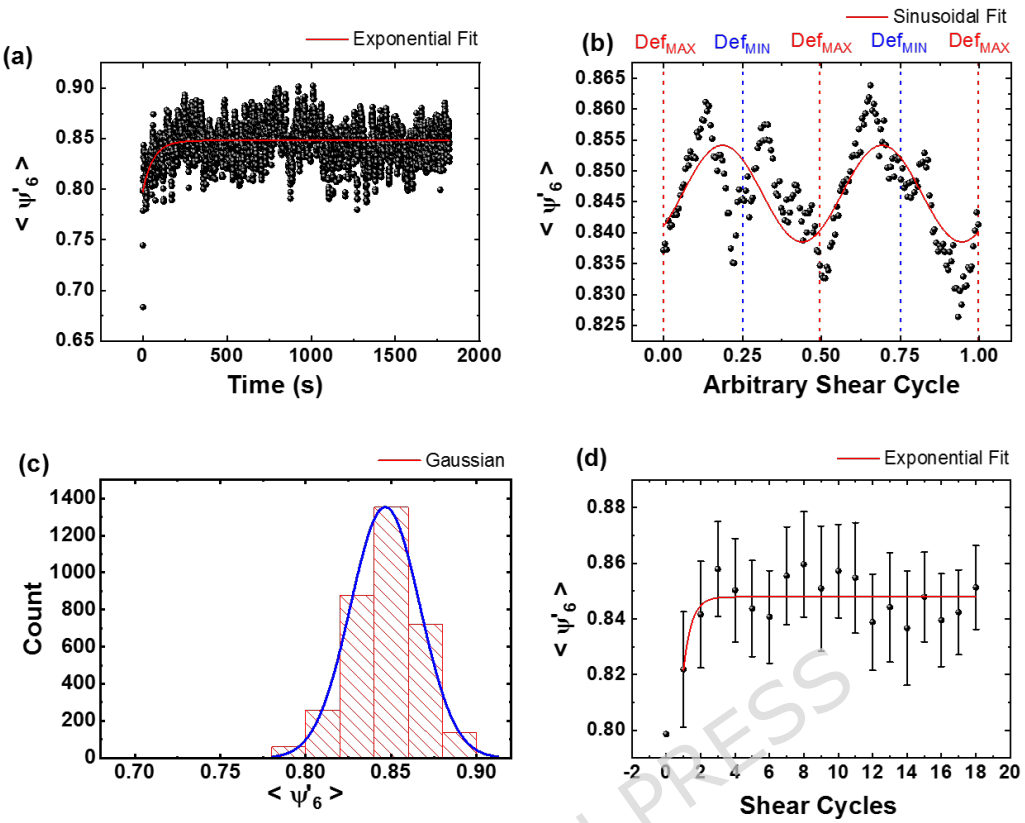

Figure 5. Statistical analysis of the sixth order bond orientational parameter for cyclic deformations at 0.01 Hz. (a) Plot of the global average $< \psi_6^{'} >$ of the ensemble measured every second throughout the entire duration of the experiment. (b) Average $< \psi_6^{'} >$ curve of the shear cycles and sinusoidal fit. (c) Histogram and normal fit. (d) Average values of $< \psi_6^{'} >$ (and standard deviations) per shear cycle and exponential fit.

the power spectrum captures scale invariance. It follows a power law, $P(f) \propto 1/f^{\beta}$, where the spectral density exponent β measures the strength of the correlations present in the time series[46]. A random non-correlated time series, $\beta = 0$, is known as white noise. For correlated series $\beta > 0$, and if $\beta = 2$, the time series is called Brownian motion[47–51]. In a previous publication, we have studied Brownian motion in a nonvibrating granular model consisting of steel balls that move by the application of an oscillating magnetic field in the z direction, which is perpendicular to the xy plane where the balls move; to characterize this system we use FA and DFA[39]. Now we apply the FA technique to the two-dimensional soft sphere granular system, with inclination, for different values of frequency in Hz.

We start by calculating the Fourier power spectrum from the time series of positions in the direction $\psi_6^{'}$, $\psi_6^{'}(i) = (\psi_{61}^{'}, \psi_{62}^{'}, ..., \psi_{6M}^{'})$, with $M = 1800$ data points. Since the time resolution is $1/60$ s, and considering sequences of 1800 observations, the duration of the time series analyzed is approximately 30 min. The corresponding Fourier power spectra of the time series of the position in the direction of the ellipsoidal particles are shown in Fig. 9. In all the cases analyzed here, when the frequency is different from 0 Hz, β is slightly greater than 1, which indicates that the system is non-stationary[50–52]. While for the case where the frequency is 0 Hz, its Fourier power spectrum $P(f) \propto 1/f^{\beta}$ with $\beta \approx 0.04$ is flat, reflecting that all frequencies contribute equally to the spectrum. If a system exhibits a time series that behaves as white noise, then the interpretation may be that the system is subjected to internal or external fluctuations that are random and uncorrelated. A time series of white noise is stationary, reflecting that statistical properties of the time series such as mean, standard deviation, etc., do not vary over time.

At this point, it is worth emphasizing the following: The Fourier analysis is used as a diagnostic tool to distinguish between stationary and non-stationary temporal behaviors in the evolution of the bond-orientational order parameter $\psi_6^{'}$ under varying

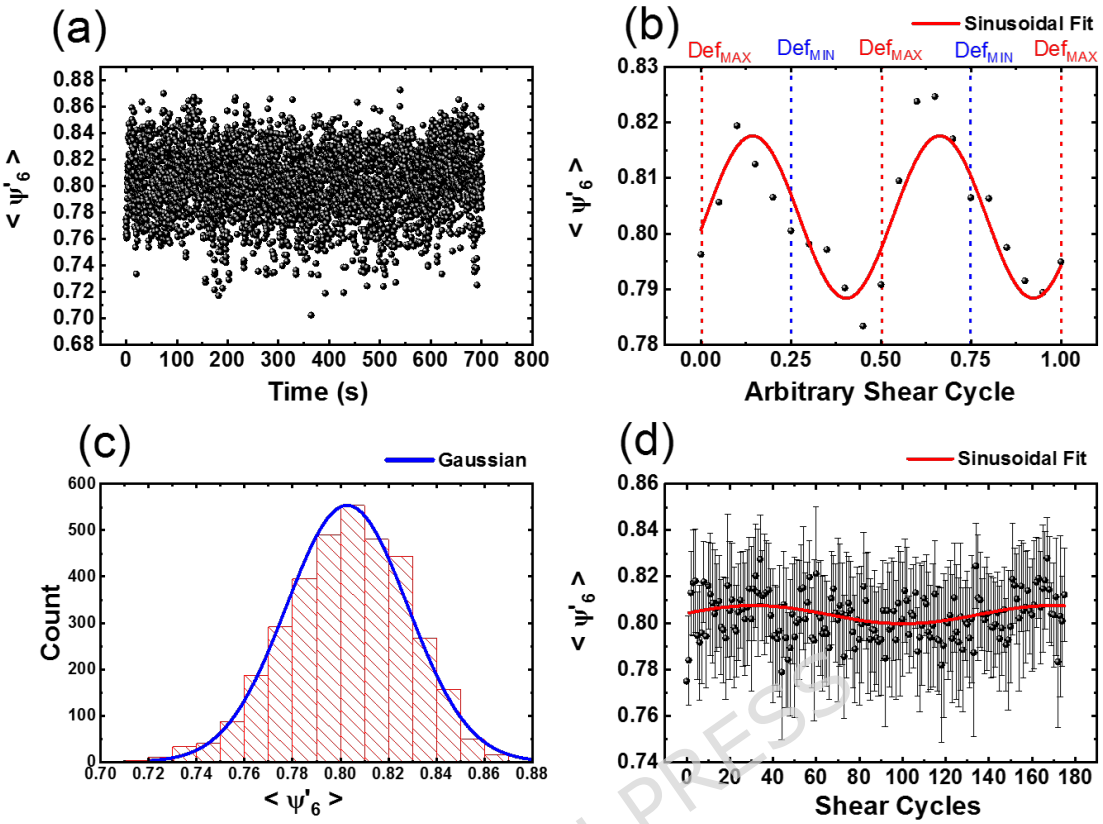

Figure 6. Statistical analysis of the sixth order bond orientational parameter for cyclic deformations at 0.25 Hz. (a) Plot of the global average $< \psi_6^{'} >$ of the ensemble measured every second throughout the entire duration of the experiment. (b) Average $< \psi_6^{'} >$ curve of the shear cycles and sinusoidal fit. (c) Histogram and normal fit. (d) Average values of $< \psi_6^{'} >$ (and standard deviations) per shear cycle and sinusoidal fit.

shear frequencies. The marked difference between the nearly flat spectrum at zero shear frequency ($\beta \approx 0.04$) and the power-law behavior for finite frequencies provides supporting evidence for the dynamic transitions observed experimentally.

Estimation of packing fraction and comparison with the jamming threshold To further characterize the structural states of the system under different shear frequencies, we estimated the two-dimensional packing fraction φ_{2D} for each condition. This quantity, also referred to as planar density, is defined as the ratio of the total area occupied by particles to the area enclosed by the system. Given that the granular assembly does not fully occupy the container during most experiments, we adopted a local definition based on the convex hull surrounding the visible particle cluster.

Each individual hydrogel particle was segmented from the recorded images and approximated as a disk of radius $r = 0.535$ cm, based on the measured diameter of 1.07 ± 0.1 cm. The occupied area was then computed as $N\pi r^2$, where $N = 534$ is the total number of particles in the system. The enclosing area was defined as the polygonal region calculated by the convex hull of the particle positions. This methodology captures the local compaction of the effective region involved in the dynamics.

Figures 10 (a)–(c) show the time evolution of the planar packing fraction φ_{2D} for three different shear frequencies: (a) 0.001 Hz, (b) 0.1 Hz, and (c) 0.25 Hz. A horizontal dashed blue line at $\varphi_{2D} = 0.9069$ indicates the theoretical hexagonal close-packed (HCP) value for two-dimensional hard disks[53]. At the lowest frequency (Fig. 10-(a)), the values of φ_{2D} fluctuate between 0.85 and 0.93, with a mean value of 0.87791. The system occasionally exceeds the HCP limit due to the softness of the hydrogel spheres, which allows for deformation and the effective disappearance of interstitial spaces. The low-frequency excitation gradually increases the effective pressure on the assembly, promoting compaction via elastic deformation of the particles. At 0.1 Hz (Fig. 10-(b)), φ_{2D} varies between 0.80 and 0.88, with a mean value of 0.83346. The increased kinetic

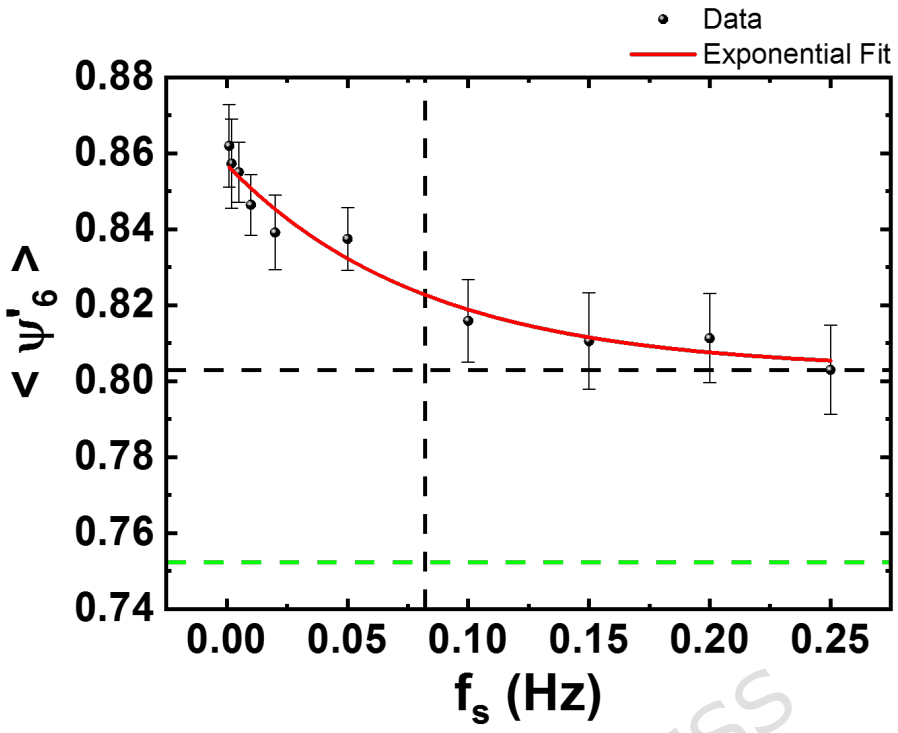

Figure 7. Average value of the orientational order parameter $\langle \psi_6' \rangle$ over the 30-minute experiment as a function of shear frequency f_s (Hz). Black dots correspond to experimental measurements, and error bars represent the standard deviation of $\langle \psi_6' \rangle$ over the measurement time. The solid red curve represents a fit using an exponential approach to a high-frequency asymptote, $\langle \psi_6' \rangle(f_s) = \langle \psi_6' \rangle_\infty + (\langle \psi_6' \rangle_0 - \langle \psi_6' \rangle_\infty) \exp(-f_s/f_c)$. The fit yields $\langle \psi_6' \rangle_\infty = 0.803 \pm 0.006$, $\langle \psi_6' \rangle_0 = 0.857 \pm 0.009$, and $f_c = 0.082 \pm 0.026$ Hz. Dashed lines indicate the asymptotic value $\langle \psi_6' \rangle_\infty$ (horizontal) and the characteristic frequency f_c (vertical). The green dashed line indicates the corresponding value for the vibrated reference system.

energy imparted by the moving boundaries induces particle rearrangements rather than deformation, reducing the system's capacity to eliminate voids. As a result, the packing fraction decreases and the structure deviates from ideal HCP order. At the highest frequency of 0.25 Hz (Fig. 10-(c)), φ_{2D} ranges from 0.77 to 0.86, with a mean of 0.81248. Under these conditions, particle motion becomes more vigorous, leading to a looser and increasingly amorphous configuration. This progression highlights a transition from a deformation-dominated regime at low frequencies—where particles accommodate space via soft compression—to a reorganization-dominated regime at higher frequencies, where increased agitation hinders hexagonal ordering despite available space. Fig. 10-(d) shows the mean planar packing fraction $\langle \varphi_{2D} \rangle$, averaged over the 30-minute experiment, as a function of the shear frequency f_s. Three horizontal dashed lines are included for reference: a blue line at $\varphi_{2D} = 0.9069$, corresponding to the hexagonal close packing (HCP) limit; a green line at $\varphi_{2D} = 0.8449$, indicating the mean packing fraction of the reference system under vibration-only conditions; and a magenta line at $\varphi_{2D} = 0.82$, representing the random close packing (RCP) threshold for hard disks in two dimensions[54,55]. A clear decreasing trend of $\langle \varphi_{2D} \rangle$ with increasing shear frequency is observed, indicating a progressive loss of structural compactness as the driving becomes faster. The data are well described by an exponential approach to a high-frequency asymptotic value,

$$\langle \varphi_{2D} \rangle(f_s) = \langle \varphi_{2D} \rangle_\infty + (\langle \varphi_{2D} \rangle_0 - \langle \varphi_{2D} \rangle_\infty) \exp(-f_s/f_c), \tag{2}$$

with fitted parameters $\langle \varphi_{2D} \rangle_\infty = 0.79 \pm 0.03$, $\langle \varphi_{2D} \rangle_0 \simeq 0.88$, and a characteristic frequency $f_c = 0.17 \pm 0.11$ Hz. The asymptotic value $\langle \varphi_{2D} \rangle_\infty$ lies close to the RCP limit, suggesting that at sufficiently high shear frequencies the system saturates into a minimally organized state dominated by random configurations. The characteristic frequency f_c defines the crossover between a low-frequency regime, where cyclic shear promotes compaction and ordering, and a high-frequency regime in which rapid driving hinders structural relaxation and leads to looser packings.

The measured values of φ_{2D} are reported in Table 1, along with their comparison to the known jamming threshold in two dimensions. For soft, deformable particles like the hydrogels used here, previous works on soft granular and particulate systems, such as bidisperse emulsions, foams, and frictionless soft disks,report a jamming point around $\varphi_J^{2D} \approx 0.84-0.85$[56–60]. While

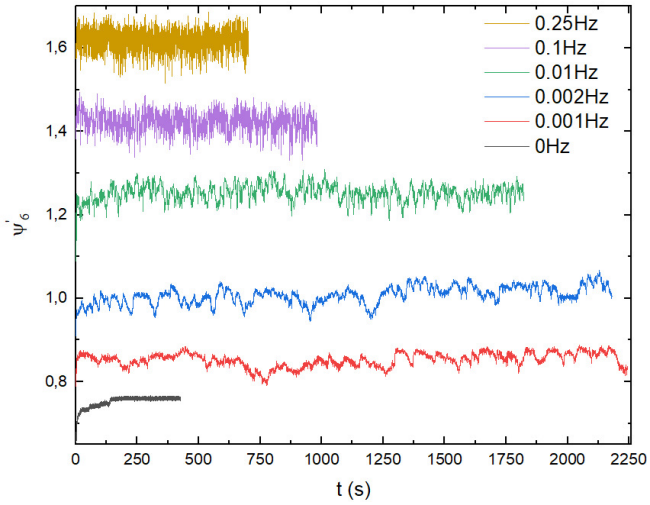

Figure 8. Representative time series of particle positions in the direction of the sixth bond orientational order parameter $\psi_6^{'}$, $\psi_6^{'}(i) = (\psi_{61}^{'}, \psi_{62}^{'}, \ldots, \psi_{6M}^{'})$; $i = 1, \ldots, M$, for several values of shear frequency.

the specific mechanical response may vary depending on particle shape, dissipation mechanisms, or confinement conditions, this range serves as a robust benchmark for marginal rigidity in soft, deformable assemblies. Although the present system is not confined in a rigid container and some edge fluctuations are present, the local packing fraction remains a reliable indicator of the collective phase. For the reference condition with vibration only and no shear, the mean packing fraction is $\varphi_{2D} = 0.8449$, falling precisely within the expected jamming range.

Table 1. Measured planar density φ_{2D} for each shear frequency and comparison with the jamming threshold $\varphi_J^{2D} \approx 0.84$.

Frequency (Hz)	φ_{2D}	Relation to φ_J^{2D}	Structural interpretation
0.001	0.87791	$> \varphi_J^{2D}$	Jammed crystalline
0.002	0.87930	$> \varphi_J^{2D}$	Jammed crystalline
0.010	0.87655	$> \varphi_J^{2D}$	Highly dense
0.050	0.87180	$> \varphi_J^{2D}$	Locally ordered
0.100	0.83346	$\approx \varphi_J^{2D}$	Transitional regime
0.150	0.82300	$< \varphi_J^{2D}$	Weakly jammed or marginal state
0.200	0.82554	$< \varphi_J^{2D}$	Onset of fluid-like behavior
0.250	0.81248	$\ll \varphi_J^{2D}$	Amorphous, unjammed

The results confirm that at low shear frequencies, the system remains in a jammed state with packing fractions clearly above the jamming point. As frequency increases, the particles gain mobility and the system transitions into less compact, disordered states. The crossover occurs around 0.1–0.15 Hz, where φ_{2D} approaches the critical jamming value.

Dynamic modulus To interpret the frequency-dependent response of the granular hydrogel system under cyclic shear, we adopt the framework of the Soft Glassy Rheology (SGR) model[61], originally introduced to describe the viscoelastic behavior of disordered soft materials such as foams, emulsions, and pastes. The SGR model is particularly suitable for systems that, while lacking thermal agitation, exhibit slow structural relaxation and history-dependent mechanical response under external driving. In our case, the vibrated hydrogel particles form a soft granular medium where structural rearrangements occur through activated dynamics under repeated shear. These features justify the application of SGR to interpret the interplay between elasticity and dissipation in our system.

A central prediction of the SGR model is that the complex shear modulus scales as $G^*(\omega) \sim \omega^{x-1}$, where x is an effective noise temperature parameter ($1 < x < 2$ in the soft glassy regime) and $\omega = 2\pi f_s$ is the angular frequency of the applied shear cycles at shear frequency f_s. This sublinear power-law behavior manifests in both the storage ($G'(\omega)$) and loss ($G''(\omega)$) moduli, reflecting the nontrivial balance between reversible elastic deformations and dissipative rearrangements in soft glasses.

Although we do not directly measure stress or strain fields, we infer the mechanical response by tracking the oscillatory behavior of the local orientational order parameter $\psi_6'(t)$ over successive shear cycles. This structural descriptor captures

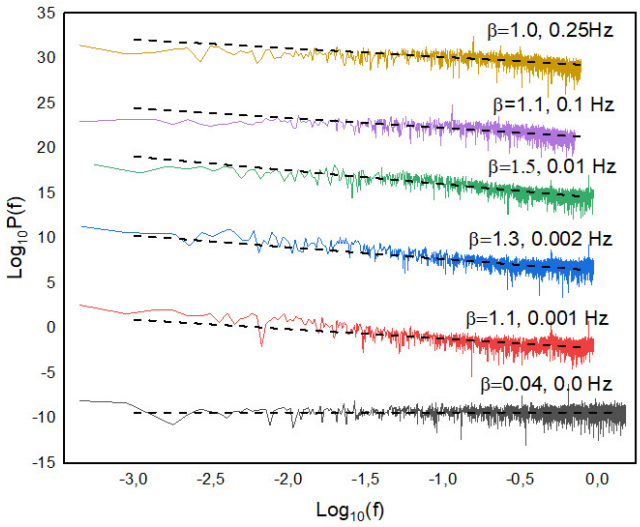

Figure 9. Fourier power spectra of the time series of the position in the direction of the sixth bond orientational order parameter ψ_6' of the two-dimensional soft sphere granular system, with inclination, for different values of shear frequency in Hz, in the same graph, the linear fits used to obtain the parameter β are shown as black dashed lines. In all the cases analyzed here, when the shear frequency is different from 0 Hz, β is slightly greater than 1, which indicates that the system is non-stationary. For the case where the frequency is 0 Hz, we have white noise since $\beta \approx 0.04$. The uncertainties in β are on the order of 0.03 in all cases, except for the case $\beta \approx 0.04$, where the uncertainty is on the order of 0.02.

the temporal evolution of bond-orientational order under deformation, and its oscillatory dynamics serve as a proxy for the viscoelastic response. For each driving frequency ω, we compute the temporal average of $\psi_6'(t)$ and fit it with a sinusoidal model at the same frequency:

$$\psi_6'(t) = A(\omega)\sin(\omega t - \delta(\omega)) + \psi_6'^{(0)}, \tag{3}$$

where $A(\omega)$ is the amplitude of the oscillation, $\delta(\omega)$ is the phase lag relative to the applied shear, and $\psi_6'^{(0)}$ is the average structural order over the cycle. These fits are shown in Figures 5-(b) and 6-(b) for the experimental cases at 0.01 and 0.25 Hz, respectively.

The amplitude $A(\omega)$ quantifies the degree of reversible structural ordering, while the phase shift $\delta(\omega)$ reflects the delay between structural response and external forcing, thus encoding both elastic and dissipative components. From these parameters, we reconstruct a complex modulus:

$$G^*(\omega) = G'(\omega) + iG''(\omega) = A(\omega)e^{i\delta(\omega)}. \tag{4}$$

Here, $G'(\omega) = A(\omega)\cos\delta(\omega)$ corresponds to the in-phase (elastic) response and $G''(\omega) = A(\omega)\sin\delta(\omega)$ to the out-of-phase (viscous) response. By plotting $G'(\omega)$ and $G''(\omega)$ versus frequency, we examine whether they exhibit sublinear power-law scaling consistent with the SGR prediction.

We applied this approach across the range of driving shear frequencies from 0.001 to 0.25 Hz, as shown in Fig. 11, where the frequency-dependent storage modulus $G'(\omega)$ and loss modulus $G''(\omega)$ are plotted on a log-log scale. The results reveal that $G'' > G'$ throughout the entire frequency range, indicating a predominantly viscous response and reflecting dissipative behavior under cyclic shear. The storage and loss moduli were then fitted with power-law models of the form $\alpha\,\omega^{\beta}$, yielding:

$$G'(\omega) = 0.031\,\omega^{0.277} \quad \text{and} \quad G''(\omega) = 0.518\,\omega^{0.109}.$$

The steeper slope of $G'(\omega)$ suggests that the material tends to become relatively more elastic at higher frequencies. From these exponents, we estimate effective noise temperatures $x = \beta + 1$, yielding $x \approx 1.277$ from G' and $x \approx 1.109$ from G'', consistent with the SGR model's prediction for soft glassy materials ($1 < x < 2$). These findings demonstrate that our granular hydrogel system exhibits rheological signatures of soft glassy materials, including sublinear frequency scaling and a combination of elastic and dissipative responses under cyclic shear within the explored shear frequency range.

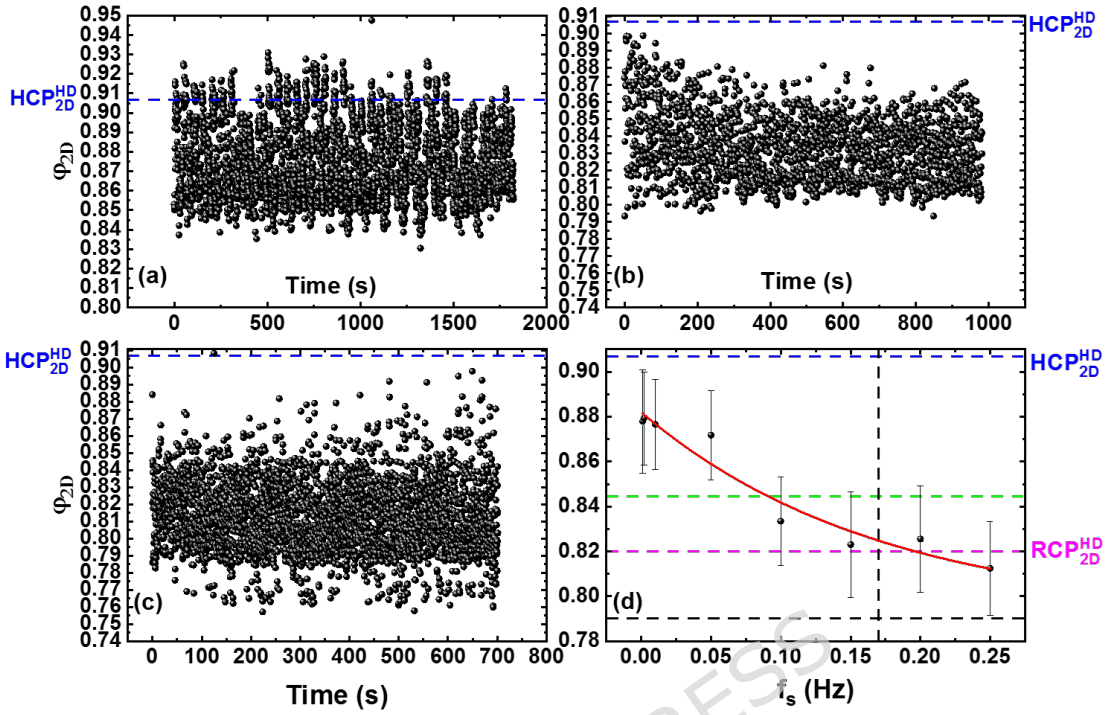

Figure 10. Time evolution and frequency dependence of the planar packing fraction φ_{2D} under increasing shear frequency. (a–c) Temporal evolution of φ_{2D} for three shear frequencies: (a) 0.001 Hz, (b) 0.1 Hz, and (c) 0.25 Hz. The dashed horizontal blue line marks the theoretical 2D hexagonal close-packed limit for hard disks HCP^{HD}_{2D}, $\varphi_{2D} = 0.9069$. (d) Mean planar packing fraction $\langle\varphi_{2D}\rangle$, averaged over the 30-minute experiment, as a function of the shear frequency f_s (Hz). Black dots correspond to experimental measurements, and error bars represent the standard deviation of $\langle\varphi_{2D}\rangle$ over the measurement time. The solid red curve represents a fit using an exponential approach to a high-frequency asymptotic value, $\langle\varphi_{2D}\rangle(f_s) = \langle\varphi_{2D}\rangle_\infty + (\langle\varphi_{2D}\rangle_0 - \langle\varphi_{2D}\rangle_\infty)\exp(-f_s/f_c)$. The fit yields $\langle\varphi_{2D}\rangle_\infty = 0.791 \pm 0.032$, $\langle\varphi_{2D}\rangle_0 = 0.882 \pm 0.031$, and $f_c = 0.171 \pm 0.112$ Hz. Dashed black lines indicate the asymptotic value $\langle\varphi_{2D}\rangle_\infty$ (horizontal) and the characteristic frequency f_c (vertical). The magenta dashed line indicates the two-dimensional random close packing limit for hard disks, $RCP^{HD}_{2D} = 0.82$, while the green dashed line corresponds to the reference vibration-only condition, $\varphi_{2D} = 0.8449$.

Dimensionless analysis of shear frequency and particle relaxation To evaluate the generality of the observed ordering-disordering transition, we consider the interplay between the externally imposed shear frequency and the intrinsic relaxation timescale of the soft granular particles. The relaxation time τ_r characterizes the typical time it takes for a particle to return to mechanical equilibrium after a small deformation, and is estimated as

$$\tau_r = \sqrt{\frac{m}{k}}, \tag{5}$$

where m is the mass of a single particle and k is the effective elastic stiffness.

Assuming the hydrogel particles are approximately spherical with radius $R \approx 0.535\,\text{cm}$ and density $\rho \approx 1000\,\text{kg}/\text{m}^3$, their mass is estimated as $m \approx \rho \frac{4}{3}\pi R^3 \approx 6.5 \times 10^{-4}\,\text{kg}$. Taking the elastic modulus of the swollen hydrogel as $E \approx 10^4\,\text{Pa}$[63], the stiffness can be approximated as $k \sim E \cdot d$, where d is the particle diameter. This yields $k \approx 107\,\text{N}/\text{m}$ and hence:

$$\tau_r \approx \sqrt{\frac{6.5 \times 10^{-4}}{107}} \approx 2.46 \times 10^{-3}\,\text{s}. \tag{6}$$

To construct a dimensionless shear frequency, we define the parameter

$$\tilde{f} = f_s \cdot \tau_r, \tag{7}$$

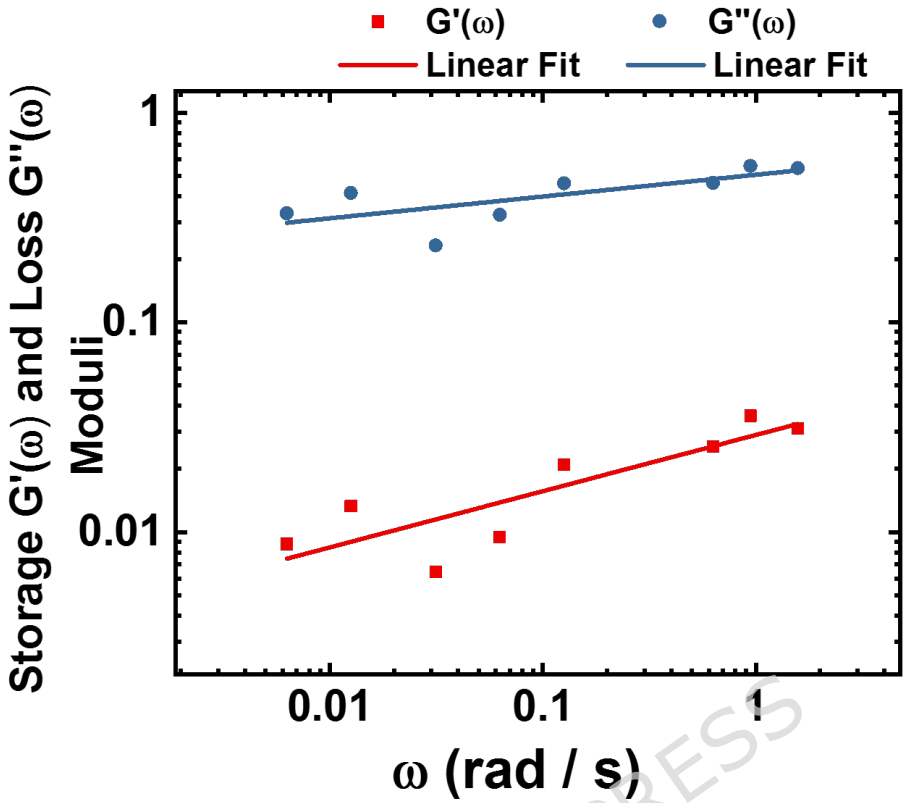

Figure 11. Frequency dependence of the storage modulus $G'(\omega)$ and the loss modulus $G''(\omega)$ plotted in log-log scale. Both moduli are extracted from the oscillatory response of the orientational order parameter $\psi_6'(t)$. Solid lines represent power-law fits (linear in log-log scale) of the form $\alpha\omega^{\beta}$, yielding $G'(\omega) = 0.031\,\omega^{0.277}$ (red line) and $G''(\omega) = 0.518\,\omega^{0.109}$ (blue line).

where f_s is the frequency of the cyclic boundary deformation. Table 2 shows the values of $\tilde{f}$ for all frequencies used in the experiment.

Table 2. Dimensionless shear frequency $\tilde{f} = f_s\tau_r$, computed using $\tau_r \approx 2.46 \times 10^{-3}$ s.

Shear frequency f_s (Hz)	Dimensionless frequency $\tilde{f}$
0.001	2.46×10^{-6}
0.002	4.92×10^{-6}
0.005	1.23×10^{-5}
0.010	2.46×10^{-5}
0.020	4.92×10^{-5}
0.100	2.46×10^{-4}
0.150	3.69×10^{-4}
0.200	4.92×10^{-4}
0.250	6.15×10^{-4}

All tested values fall well within the regime $\tilde{f} \ll 1$, where the shear cycles are slow compared to the particle relaxation timescale. This indicates that the experiments are conducted in a predominantly quasi-static regime, well separated from inertial or resonance-driven dynamics. This supports the interpretation that at low $\tilde{f}$, particles have sufficient time to dissipate and rearrange into ordered structures, leading to mechanical annealing. In this context, $\tilde{f}$ does not mark a sharp dynamic crossover at $\tilde{f} \sim 1$, but rather quantifies the degree of timescale separation between external driving and particle-level relaxation. Even in a hypothetical regime approaching $\tilde{f} \sim 1$, the strongly damped and viscoelastic nature of hydrogel contacts suggests that the dominant effect would be incomplete viscoelastic relaxation rather than the onset of inertial particle dynamics. As $\tilde{f}$ increases, the external driving becomes comparable to the intrinsic response time, suppressing local rearrangements and

promoting disorder.

While the particle relaxation time is not tunable in this experiment, the dimensionless parameter $\tilde{f}$ provides a physically motivated reference scale that could allow comparison with other systems or simulations where material stiffness or mass varies. We emphasize, however, that alternative definitions incorporating collective or viscoelastic relaxation times may become relevant in regimes closer to dynamical crossover conditions. Furthermore, the use of $\tilde{f}$ highlights the relevance of internal timescales in the transition from amorphous to ordered states under cyclic shear.

This adimensional framework also enables direct comparison with other driven particulate systems. For example, in oscillatory shear experiments on Brownian hard-sphere colloids, Nakamura et al.[5,6] identified a narrow driving-frequency window ($\tilde{f}$ defined with the diffusive time) that maximizes crystallization via cage-rattling dynamics. In contrast, in the present athermal hydrogel system, rearrangements are governed by contact elasticity and viscoelastic relaxation, with τ_r providing a natural particle-level reference timescale. While both systems exhibit enhanced ordering within specific frequency ranges, the underlying activation mechanisms differ fundamentally: thermal activation in colloids versus mechanically mediated relaxation in our hydrogels. This comparison highlights the usefulness—and the limitations—of $\tilde{f}$ as a common dimensionless descriptor across thermally and mechanically driven particulate media.

Frequency–strain phase diagram of orientational order We decided to explore at a preliminary stage how the combined effect of shear frequency and shear strain influences the orientational ordering in the system. Here, the shear strain corresponds to the imposed maximum angular deformation γ_{max} of the confining frame, as defined in the Methods section. For this purpose, we constructed a phase diagram based on the average value of the local hexagonal order parameter ψ_6', obtained from 58 experimental conditions covering a range of shear frequencies and strains. Each data point represents the steady-state average of ψ_6' after sufficient annealing cycles, reflecting the degree of hexagonal order achieved under the corresponding shear conditions. We interpolated the discrete experimental data over a fine grid to visualize the continuous variation of $\langle\psi_6'\rangle$ across the parameter space. Specifically, the scattered values of $\langle\psi_6'\rangle$ were first mapped onto the frequency–strain plane using Delaunay triangulation, which provides a robust framework for interpolating irregularly spaced data. The resulting surface, shown in Fig. 12, was then smoothed using a cubic method to produce a continuous contour plot, highlighting trends and local maxima in orientational order. While the precise location of these local maxima may vary slightly due to experimental fluctuations and finite sampling, the emergence of an intermediate frequency–strain window with enhanced orientational order is a robust trend observed across independent experimental runs. We emphasize that this interpolation is intended solely as a guide to the eye to visualize global trends, rather than to define sharp phase boundaries or fine structural features.

The phase diagram shows that orientational order is promoted within a specific band of intermediate frequencies and strains, defined by $\psi_6' > 0.85$. Outside this regime, either at intermediate frequencies and low strains, where shear is insufficient to overcome local energy barriers, so that particles remain trapped within persistent cages and cooperative rearrangements are suppressed, or at high values, where shear tends to disrupt local arrangements, the system exhibits a significant reduction in hexagonal ordering. The boundaries between regions of high and low orientational order are highlighted by dashed contours at the threshold value $\psi_6' = 0.85$. This threshold was chosen empirically to mark the onset of substantial hexagonal order.

The emergence of a band of optimal orientational order at intermediate strains can be understood by considering the balance between structural reorganization and disruption. At low strains, the applied shear is too weak to effectively mobilize particles trapped in disordered configurations, leading to limited rearrangements and hence a poor development of hexagonal domains. In contrast, at very high strains, the strong displacements induced by shear continuously disrupt already formed local structures, preventing the stabilization of long-range orientational order. Therefore, an intermediate shear strain provides the necessary mobility for particles to explore new configurations while maintaining enough stability to allow the development of ordered domains. Boundary conditions also play a role in shaping this optimal regime: in the present deformable confinement, the walls influence stress transmission and can act as preferential sites for the nucleation and alignment of ordered domains, thereby affecting the strain range over which annealing is most effective. While the existence of an optimal annealing window is thus expected to be generic for such soft systems, its precise position in strain space may shift for different confinement geometries or more compliant boundaries. We acknowledge that a denser sampling of shear strains, particularly around intermediate values such as $\gamma_{max} \approx 0.16$ rad, would further strengthen the phase diagram and clarify the boundaries of this optimal regime, and we leave this refinement for future work.

Interestingly, the diagram also shows that at sufficiently low frequencies, even small shear strains can promote hexagonal ordering. This suggests that slow deformations allow the system to respond quasi-adiabatically to the driving, giving particles enough time to rearrange cooperatively and relax into energetically favorable configurations. In this regime, the shear acts more like a gentle annealing mechanism rather than a source of disruption, regardless of its magnitude. This behavior is reminiscent of thermal and mechanical annealing processes, where order emerges not simply by increasing energy input, but by tuning the rate at which it is applied. In the same way that slow cooling in thermal annealing allows defects to be eliminated and crystalline order to emerge, low-frequency shear enables the granular system to reorganize progressively toward

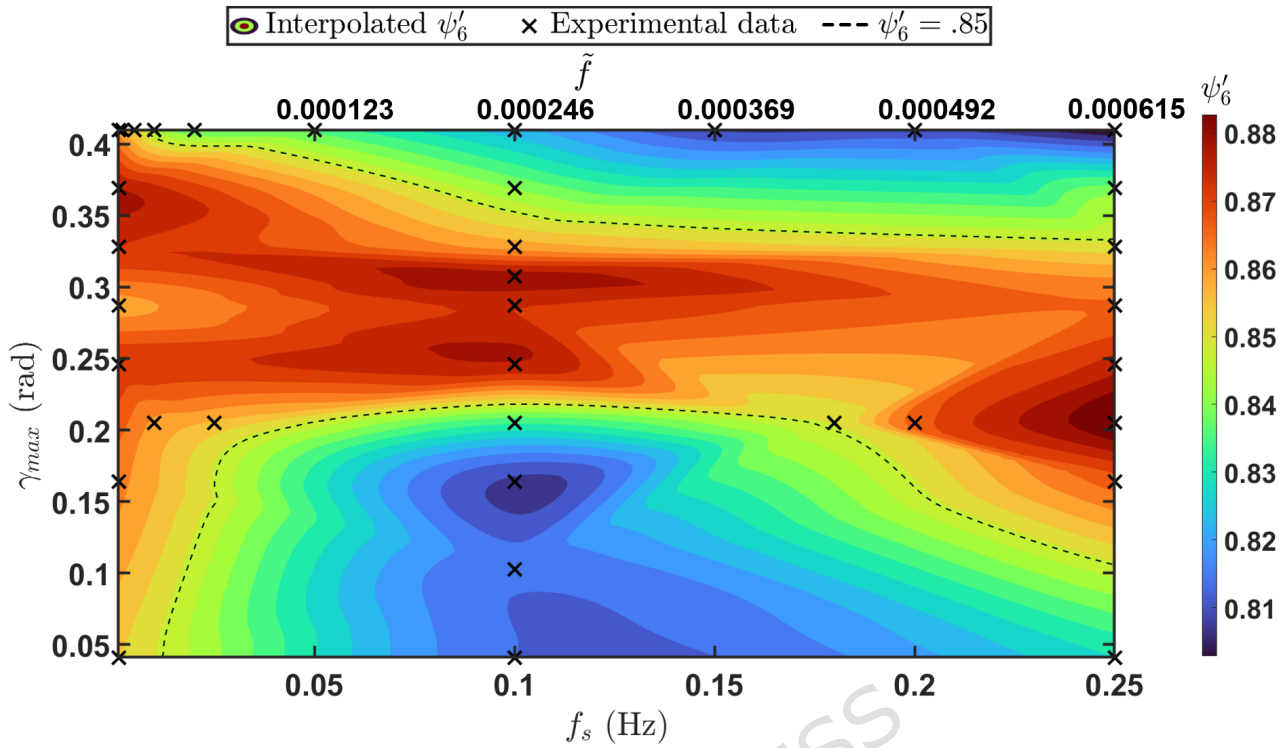

Figure 12. Phase diagram of the orientational order parameter ψ_6' as a function of shear frequency f_s and shear strain γ_{max}. 58 experimental measurements (black crosses) were interpolated using cubic interpolation over a regular mesh. The interpolation is intended solely as a guide to the eye to highlight global trends and does not imply sharply defined phase boundaries. The color map indicates the interpolated values of ψ_6', with dashed black lines denoting contour levels at 0.85, which define a region of high hexagonal order. A secondary horizontal axis indicates the corresponding dimensionless frequency $\tilde{f} = f_s \tau_r$.

hexagonal packing. Conversely, excessively fast or large shear strains continuously drive the system away from locally stable configurations, forcing it to explore new regions of the energy landscape. Rather than kinetically freezing the structure, strong deformations promote persistent disorder by repeatedly disrupting emerging ordered domains before they can stabilize. The interplay between drive frequency, strain, and internal relaxation times thus plays a central role in controlling the ordering pathways in out-of-equilibrium granular materials. Finite-size effects also play a role in this process: grain growth and domain coalescence are constrained by the finite container dimensions, and interactions with the confining boundaries can limit the maximum domain size and bias orientational alignment. While these effects may influence the quantitative position of the ordering maximum, they do not alter the qualitative trends observed in the phase diagram. The diagram includes a secondary axis showing the dimensionless frequency $\tilde{f} = f_s \tau_r$, which may provide additional insight into the relative importance of shear rate compared to the system's intrinsic relaxation time.

We stress that the main conclusions reported here rely on directly measured data, which reveal a non-monotonic dependence of orientational order on shear strain. At fixed frequency, a pronounced maximum in $\langle \psi_6' \rangle$ is observed at intermediate $\gamma_{\max}$, exceeding the associated statistical fluctuations. To quantify experimental variability and assess the robustness of this trend, we report representative error bars for $\langle \psi_6' \rangle$ (e.g., at $f_s = 0.1$ Hz), where the standard deviation is computed from steady-state time-series fluctuations evaluated over a 1000 s time window (see Fig. 13). This provides a direct estimate of the uncertainty associated with individual data points in the phase diagram. The phase diagram therefore offers a compact summary of experimentally observed trends, while the interpolation serves solely as a guide to the eye and does not affect the qualitative conclusions. Future work will focus on obtaining a denser sampling of the parameter space to further validate and refine these observations.

Conclusions and remarks

We have experimentally investigated the structural and rheological response of a vibrated granular hydrogel assembly subjected to cyclic shear at varying frequencies. Our findings reveal a rich interplay between vibrational relaxation and shear-induced reorganization arising from a competition between ordering and disordering mechanisms. Ordering emerges from vibration-

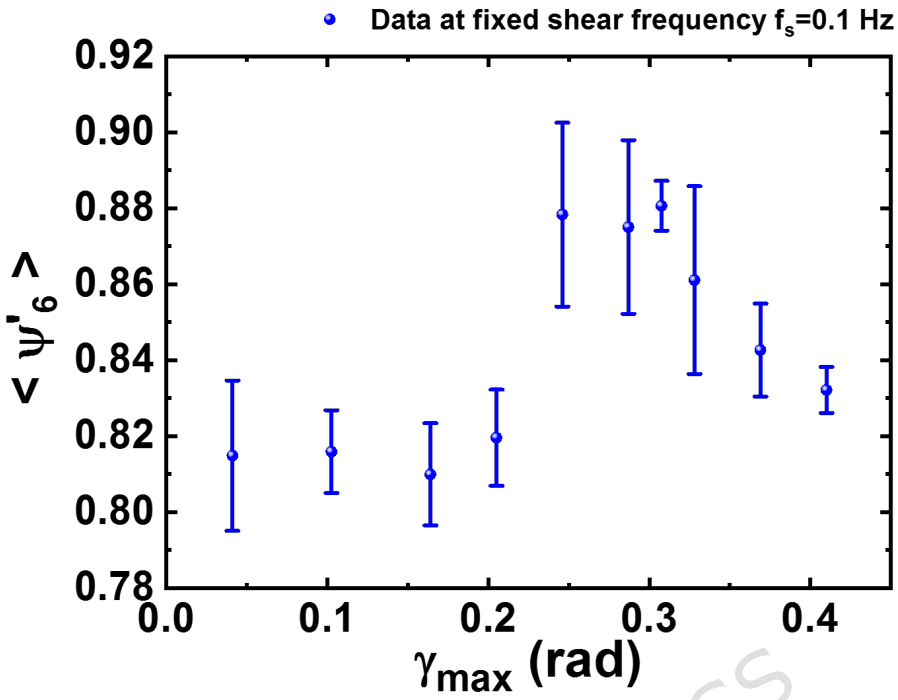

Figure 13. Average orientational order $\langle \psi' 6 \rangle$ as a function of shear strain γmax at fixed shear frequency $f_s = 0.1$ Hz. Error bars represent the standard deviation of ψ_6' computed from steady-state time series over a time window of 1000 s. The non-monotonic behavior highlights the existence of an optimal annealing window at intermediate strain amplitudes.

induced relaxation and, under certain conditions, from shear-assisted annealing. In contrast, disorder is promoted by shear-induced structural disruption and kinetic fluidization.

In the absence of shear, the system exhibits slow structural relaxation toward partial hexagonal order, driven by vibration and gravity. This baseline evolution highlights the role of gravitational asymmetry in guiding local crystallization and sets a reference for subsequent shear-driven dynamics. Upon applying cyclic shear, the competition between mechanical disruption and reordering becomes apparent. At low frequencies, deformation is slow enough to allow cooperative rearrangements and annealing of ordered domains. As the frequency increases, the imposed timescale becomes comparable to the internal relaxation time of the particles, limiting the system's ability to reorganize and ultimately suppressing long-range order.

This transition is quantitatively captured through a dimensionless shear frequency $\tilde{f} = f_s \cdot \tau_r$, which compares the driving frequency to the particle's elastic relaxation time. All experimental conditions explored here fall within the regime $\tilde{f} \ll 1$, yet a clear structural crossover is observed: from compact, ordered configurations at low $\tilde{f}$, to fluid-like, disordered states at higher values. Importantly, this crossover should not be interpreted as an inertial transition at $\tilde{f} \sim 1$, but rather as a gradual loss of quasi-static relaxation as the driving period becomes insufficient for complete particle-level viscoelastic relaxation. The decline in both orientational order and packing fraction with increasing frequency signals a shear-tunable transition across the jamming threshold. Although our current range does not access the high-frequency regime ($\tilde{f} \gg 1$) where inertial effects and dynamic shear banding may emerge, extending the experimental space into this regime represents a promising avenue for future work, potentially revealing new dynamical ordering and disordering mechanisms.

Fourier analysis of the structural time series (ψ_6') reveals a dynamic signature of this transition: from stationary ($\beta \approx 0.04$), uncorrelated fluctuations under vibration alone, to power-law spectral behavior ($\beta > 1$) under shear, consistent with history-dependent dynamics and long-range temporal correlations. This crossover indicates that cyclic shear not only restructures the material spatially, but also drives it into non-equilibrium dynamical regimes.

Finally, the system exhibits rheological behavior characteristic of soft glassy materials, as described by the Soft Glassy Rheology (SGR) model. By tracking the sinusoidal response of the local bond-orientational order, we extract complex shear moduli that scale sublinearly with frequency: $G'(\omega) \sim \omega^{0.277}$ and $G''(\omega) \sim \omega^{0.109}$. The predominance of the loss modulus over the storage modulus reflects the dissipative nature of the medium, while the increasing slope of G' suggests enhanced elasticity at higher driving rates. These rheological signatures, along with effective noise temperature estimates within the soft

glassy regime, support the interpretation of our granular hydrogel as soft glassy matter.

Complementing our structural and rheological analysis, the frequency–strain phase diagram of orientational order offers a broader perspective on how the interplay between shear strains and frequency governs the emergence of hexagonal order. This diagram reveals a well-defined regime of enhanced ordering at intermediate strains and frequencies, where shear efficiently mobilizes particles without overwhelming the system's capacity to reorganize. Interestingly, the diagram also highlights that even minimal shear strains can induce ordering at low frequencies, consistent with a quasi-adiabatic annealing mechanism. These findings emphasize that not only the magnitude but also the rate of deformation critically influences structural outcomes. By mapping these regimes, the phase diagram serves as a practical guide for tuning mechanical inputs to steer soft granular materials toward desired states of order or fluidization, reinforcing the central role of drive–relaxation balance in nonequilibrium self-organization.

Altogether, our results provide a coherent experimental picture of how soft granular assemblies respond to external forcing, bridging structural evolution, rheology, and temporal dynamics. The combination of dimensional analysis, structural metrics, and rheological proxies offers a consistent interpretative approach to probe nonequilibrium transitions in disordered soft matter systems driven by competing mechanical inputs, within the limits of the explored parameter space.

We emphasize that the present study is subject to several limitations. First, the explored frequency range is restricted to the low-frequency regime ($\tilde{f} \ll 1$), preventing access to higher frequencies where inertial effects, dynamic shear banding, or new ordering mechanisms may emerge. Second, the frequency–strain phase diagram is interpolated from a finite set of discrete conditions and does not imply sharp phase boundaries. Third, the reported rheological moduli are effective, structure-based proxies inferred from orientational order dynamics rather than direct stress measurements. Finally, the behavior is specific to soft hydrogel particles under the present driving and boundary conditions and may not generalize directly to stiffer or frictional granular materials.

Nevertheless, the observed trends provide valuable insight into the balance between shear-induced disruption and annealing-driven ordering in soft granular systems. Looking ahead, several important questions remain open and define promising directions for future work. Key extensions include exploring the high-frequency regime ($\tilde{f} \gg 1$), systematically varying particle stiffness, viscoelasticity, and shape, and modifying boundary conditions to distinguish bulk-driven ordering from boundary-induced effects. At a microscopic level, direct observation of particle-scale rearrangements is needed to link the structural and spectral signatures to elementary plastic events and cooperative dynamics. Such extensions will be essential to test the robustness of the mechanisms identified here and to assess their broader applicability across driven disordered materials.

Methods

The soft sphere granular system is composed of 534 super absorbent polyacrylamide-based hydrogel balls, each with a diameter of 1.07 ± 0.1 cm ,which are considered soft in a relative sense owing to their low elastic modulus ($\sim$ 1–200kPa) and compliant, highly hydrated polymer network[62]. Each sphere retains $0.65 \pm 0.001\, cm^3$ of water releasing it with an average speed of $-0.015 \pm 0.004\, cm^3/h$. At this release rate, it is possible to perform experiments of approximately 30 minutes and consider any mass loss of the system negligible. These particles are composed of a polyacrylamide-based hydrogel with mechanical properties comparable to single-network (SN) PAAm gels. Based on previous studies[63], we estimate a Young's modulus on the order of $E \sim 10^4$ Pa for fully swollen particles, which corresponds to the low-stiffness regime relevant to slow granular relaxation. This estimation is consistent with mechanical measurements for SN polyacrylamide gels undergoing compression. The granular sample is confined within a deformable rectangular frame. The dimensions of the frame, when in rectangular shape, are 290 mm wide and 260 mm high. Periodic deformations of the frame provide shear to the granular system. The surface, where the two-dimensional monolayer of spheres rests, is rigidly bonded to a 6.5 inch Kenwood speaker used to vibrate the system with a sinusoidal signal $A \sin(2\pi f t)$ with fixed frequency $f = 126.5 Hz$ and fixed amplitude $A \approx 0.025$ mm, to obtain a constant quotient between the peak acceleration and gravity $\Gamma \equiv A\omega^2/g = 4A\pi^2 f^2/g \approx 1.6$. The entire system is slightly tilted forming an angle $\alpha = 2.89 \pm 0.1^\circ$ with the horizontal. These conditions allow the particles to slide over the slightly inclined surface and settle to the bottom of the container due to the effect of gravity and vibration. Because of this, a partially order is reached through sedimentation that will subsequently increase with shear cycles. Deformation of the rectangular frame is achieved with its 4 corners serving as movable pivots, by fixing two additional pivots and using a linear actuator (POLOLU Model LACT2P-12V-20) with the piston connected to one corner of the frame. The input signal used in the linear actuator was a square wave whose change in voltage polarity determines a cyclic deformation. A schematic of the experimental system is shown in Fig. 14-(a). To quantify the angular deformation of the frame provoked by the stroke of the piston, we consider an angular parameter $\gamma(t)$ defined as the angle showed in Figs. 14-(b) and (c) where $|\gamma(t)| < \gamma_{max}$. The effects of shear frequency were studied. For this purpose, the shear strain was fixed at 0.41 rad (approximately 23.5°), and the following frequencies were selected: 0.001, 0.002, 0.005, 0.01, 0.02, 0.1, 0.15, 0.2, and 0.25 Hz. We record runs of around 30 minutes of video, which corresponds to two shear cycles for the lowest frequency of 0.001 Hz. The configurational order was

evaluated using the sixth bond-orientational order parameter, denoted as ψ_6'. This parameter is defined by the expression:

$$\psi_6' = \frac{1}{N_B}\left|\sum_{j=1}^{N_B} e^{(i6\theta_j)}\right|, \quad 0 \le \theta_j < 2\pi \tag{8}$$

where θ_j represents the angle formed by the bond between a reference particle and its nearest neighbors j in relation to an arbitrary axis. Here, N_B is determined through Delaunay triangulation along with a cutoff criterion based on a specified distance equal to one effective diameter[37,41].

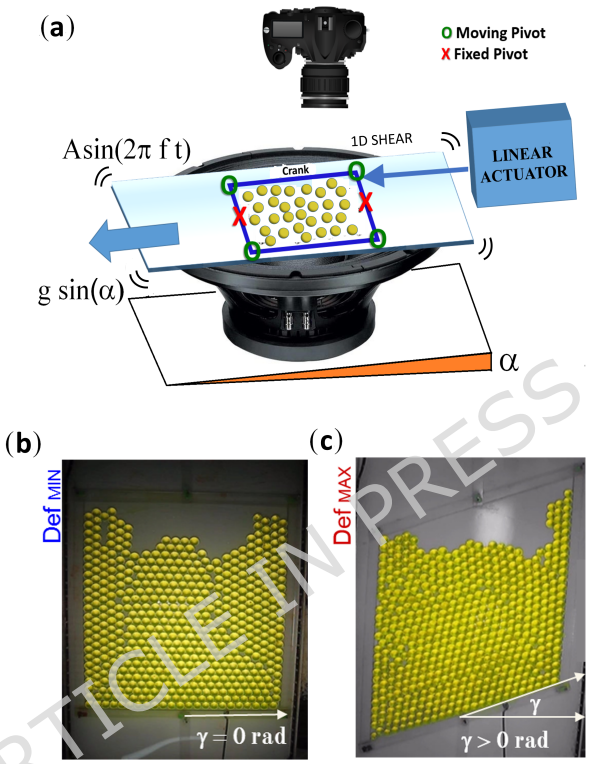

Figure 14. (a) Schematic of the experimental setup: a deformable frame enclosing a two-dimensional hydrogel granular sample is mounted on a slightly inclined vibrating surface. Shear is induced by deforming the frame using a linear actuator. (b) and (c) Photographs of the deformable frame at (b) its minimum deformation, $\gamma = 0$ rad, and (c) one of its maximum deformations, when $\gamma = |\gamma_{\max}| = 0.41$ rad.

References

1. López-González, F., Herrera-González, A. M. & Donado, F. Study of the transition from amorphous to crystalline phase in a granular system under shearing and vibration. *Phys. A* **590**, 126756 (2022).
2. López-González, F., Pacheco-Vázquez, F. & Donado, F. Ordering of a granular layer of cubes under strain-induced shear and vibration. *Phys. A* **620**, 128768 (2023).
3. Rietz, F., Radin, C., Swinney, H. L. & Schröter, M. Nucleation in sheared granular matter. *Phys. Rev. Lett.* **120**, 701 (2018).
4. Panaitescu, A., Reddy, K. A. & Kudrolli, A. Nucleation and crystal growth in sheared granular sphere packings. *Phys. Rev. Lett.* **108** (2012).
5. Nakamura, N., Inayama, K., Okuno, T., Ogi, H. & Hirao, M. Accelerated crystallization of colloidal glass by mechanical oscillation. *Scientific Reports* **7**(1), 13699 (2017).
6. Nakamura, N., Nakashima, S. & Ogi, H. Mechanical oscillation accelerating nucleation and nuclei growth in hard-sphere colloidal glass. *Scientific Reports* **9**, 12836 (2019).
7. Morales-Barrera, D., Rodríguez-Gattorno, G. & Carvente, O. Reversible self-assembly (fcc-bct) crystallization of confined granular spheres via a shear dimensionality mechanism. *Phys. Rev. Lett.* **7**, 121 (2018).
8. Daniels, K. E. & Behringer, R. P. Hysteresis and competition between disorder and crystallization in sheared and vibrated granular flow. *Phys. Rev. Lett.* **94**, 168001 (2005).
9. Asencio, K., Acevedo, M., Zuriguel, I. & Maza, D. Experimental study of ordering of hard cubes by shearing. *Phys. Rev. Lett.* **119**, 228002 (2017).
10. Smith, P. A., Petekidis, G., Egelhaaf, S. U. & Poon, W. C. K. Yielding and crystallization of colloidal gels under oscillatory shear. *Phys. Rev. E* **76**, 4 (2007).
11. Qi-Cheng, S. Granular structure and the nonequilibrium thermodynamics. *Wuli Xuebao* **64**(7), 076101 (2015).
12. Bloom, M., Russell, M., Kustau, A., Mandayam, S. & Sukumaran, B. An X-ray computed tomography technique for the measurement of packing density in granular particles. *2009 IEEE Instrumentation and Measurement Technology Conference*, 978–983 (2009).
13. Xing, Y., Zheng, J., Li, J., Cao, Y., Pan, W., Zhang, J. & Wang, Y. X-ray tomography investigation of cyclically sheared granular materials. *Phys. Rev. Lett.* **126**, 048002 (2021).
14. Radhakrishnan, R. & Fielding, S. M. Shear banding in large amplitude oscillatory shear (LAOStrain and LAOStress) of soft glassy materials. *J. Rheol.* **62**, 559–576 (2018).
15. Møller, P. C. F., Rodts, S., Michels, M. A. J. & Bonn, D. Shear banding and yield stress in soft glassy materials. *Phys. Rev. E* **77**, 041507 (2008).
16. Fielding, S. M. Shear banding in soft glassy materials. *Rep. Prog. Phys.* **77**, 102601 (2014).
17. Yu, A. B., An, X. Z., Zou, R. P., Yang, R. Y. & Kendall, K. Self-assembly of particles for densest packing by mechanical vibration. *Phys. Rev. Lett.* **97**, 265501 (2006).
18. Ciamarra, S. M. P., Coniglio, A., De Martino, D. & Nicodemi, M. Shear- and vibration-induced order-disorder transitions in granular media. *Eur. Phys. J. E* **24**, 411-415 (2007).
19. Otsuki, M. & Hayakawa, H. Universal scaling for the jamming transition. *Prog. Theor. Phys.* **121**, 647–652 (2009).
20. Dai, W., Reimann, J., Hanaor, D., Ferrero, C. & Gan, Y. Modes of wall induced granular crystallisation in vibrational packing. *Granular Matter* **21**, 2 (2019).
21. Jin, W., O'Hern, C. S., Radin, C., Shattuck, M. D. & Swinney, H. L. Homogeneous crystallization in cyclically sheared frictionless grains. *Phys. Rev. Lett.* **125**, 258003 (2020).
22. Athanassiadis, A. G., Miskin, M. Z., Kaplan, P., Rodenberg, N., Lee, S. H., Merritt, J., Brown, E., Amend, J., Lipson, H. & Jaeger, H. M. *Particle shape effects on the stress response of granular packings*. Soft Matter **10**, 48–59 (2014).
23. Frenkel, D., Mulder, B. M. & McTague, J. P. Phase diagram of hard ellipsoids of revolution. *Mol. Cryst. Liq. Cryst.* **123**, 119–128 (1985).
24. Shakya, C., van der Gucht, J. & Dijksman, J. A. Viscoelastic material properties determine the contact mechanics of hydrogel spheres. *Front. Phys.* **12**, 1334325 (2024).
25. Basu, A. et al. Rheology of soft colloids across the onset of rigidity: scaling behavior, thermal, and non-thermal responses. *Soft Matter* **10**, 3027–3035 (2014).

26. Tapia, F., Hong, C.-W., Aussillous, P. & Guazzelli, É. Rheology of suspensions of non-Brownian soft spheres across the jamming and viscous-to-inertial transitions. *Phys. Rev. Lett.* **133**, 088201 (2024).

27. Vialetto, J., Ramakrishna, S. N., Isa, L. & Laurati, M. Effect of particle stiffness and surface properties on the non-linear viscoelasticity of dense microgel suspensions. *J. Colloid Interface Sci.* **672**, 814–823 (2024).

28. Yang, R., Bernardino, K., Xiao, X., Gomes, W. R., Mattoso, D. A., Kotov, N. A., Bogdan, P. & de Moura, A. F. Graph theoretical description of phase transitions in complex multiscale phases with supramolecular assemblies. *Adv. Sci.* **11**, e2402464 (2024).

29. Taghizadeh, K., Luding, S., Basak, R. & Kondic, L. Understanding slow compression of frictional granular particles by network analysis. *Soft Matter* **20**, 6440–6457 (2024).

30. Luding, S., Taghizadeh, K., Cheng, C. & Kondic, L. Understanding slow compression and decompression of frictionless soft granular matter by network analysis. *Soft Matter* **18**, 1868–1884 (2022).

31. Fiocco, D., Foffi, G. & Sastry, S. Encoding of memory in sheared amorphous solids. *Phys. Rev. Lett.* **112**, 025702 (2014).

32. Kawasaki, T. & Berthier, L. Macroscopic yielding in jammed solids is accompanied by a nonequilibrium first-order transition in particle trajectories. *Phys. Rev. E* **94**, 022615 (2016).

33. Liu, C., Dutta, S., Chaudhuri, P. & Martens, K. Elastoplastic approach based on microscopic insights for the steady state and transient dynamics of sheared disordered solids. *Phys. Rev. Lett.* **126**, 138005 (2021).

34. Seto, R., Singh, A., Chakraborty, B., Denn, M. M. & Morris, J. F. Shear jamming and fragility in dense suspensions. *Granular Matter* **21**, 93 (2019).

35. Royall, C. P., Poon, W. C. K. & Weeks, E. R. In search of colloidal hard spheres. *Soft Matter* **9**, 1 (2013).

36. Steinhardt, P., Nelson, D. & Ronchetti, M. Bond-orientational order in liquids and glasses. *Phys. Rev. B* **28**, 784 (1983).

37. Mickel, W., Kapfer, S. C., Schröder-Turk, G. & Mecke, K. Shortcomings of the bond orientational order parameters for the analysis of disordered particulate matter. *J. Chem. Phys.* **138**, 044501 (2013).

38. Torres-Vargas, G., Fossion, R., Donado, F., López-González, F. & Tapia-Ignacio, C. Scale invariance in a nonvibrating magnetic granular system. *Scientific Reports* **10**, 11474 (2020).

39. Torres-Vargas, G., Tapia-Ignacio, C., Donado, F., Fossion, R. & Santiago, J. A. Emergence of scale invariance in the dynamics of an ellipsoidal particle on a granular magnetic bath. *Phys. A* **572**, 125903 (2021).

40. Fossion, R., Donado, F., Jaguey-Hernández, Y. & Tapia-Ignacio, C. Application of Fourier analysis to an ellipsoidal particle on a granular magnetic bath. *Phys. A* **630**, 129258 (2023).

41. Delaunay, B. Sur la sphère vide. *Bulletin de l'Académie des Sciences de l'URSS, Classe Sci. Math. Nat.* **6**, 793–800 (1934).

42. Sbalzarini, I. F. & Koumoutsakos, P. Feature point tracking and trajectory analysis for video imaging in cell biology. *J. Struct. Biol.* **151**, 182-195 (2005).

43. García-Iglesias, L., Rivera, A. L. & Fossion, R. Circadian cycles: A time-series approach. *Rev. Mex. Fis.* **69**, 051101 (2023).

44. Koopmans, L. H. *The Spectral Analysis of Time Series*, Vol. 22 (Academic Press, 1995).

45. Bloomfield, P. *Fourier Analysis of Time Series: An Introduction*, Vol. 2 (John Wiley and Sons, 2000).

46. Fossion, R., Landa, E., Stránský, P., Velázquez, V., López-Vieyra, J., Garduño, I., García, D. & Frank, A. Scale invariance as a symmetry in physical and biological systems: Listening to photons, bubbles and heartbeats. *AIP Conference Proceedings* **1323**, 74-90 (2010).

47. Addison, P. S. *Fractals and Chaos: An Illustrated Course*, First ed. (IOP Publishing Ltd, 1997).

48. Eke, A., Hermán, P., Bassingthwaighte, J., Raymond, G., Percival, D., Cannon, M., Balla, I. & Ikrényi, C. Physiological time series: Distinguishing fractal noises from motions. *Pflugers Arch.* **439**, 403-415 (2000).

49. Eke, A., Herman, P., Kocsis, L. & Kozak, L. R. Fractal characterization of complexity in temporal physiological signals. *Physiol. Meas.* **23**, R1-38 (2002).

50. Halley, J. M. & Inchausti, P. The increasing importance of 1/f-noises as models of ecological variability. *Fluctuation and Noise Letters* **4**, R1-R26 (2004).

51. Su, Z. Y. & Wu, T. Music walk, fractal geometry in music. *Phys. A* **380**, 418-428 (2007).

52. Halley, J. M. Ecology, evolution and 1f-noise. *Trends in Ecology & Evolution* **11**, (1):33-37 (1996).

53. Torquato, S. & Stillinger, F. H. Jammed hard-particle packings: From Kepler to Bernal and beyond. *Rev. Mod. Phys.* **82**, 2633–2672 (2010).

54. Atkinson, S., Stillinger, F. H. & Torquato, S. Existence of isostatic, maximally random jammed monodisperse hard-disk packings. *Proc. Natl. Acad. Sci. U. S. A.* **111**, 18436–18441 (2014).

55. Brouwers, H. J. H. A geometric probabilistic approach to random packing of hard disks in a plane. *Soft Matter* **19**, 8465–8471 (2023).

56. Reichhardt, C. & Reichhardt, C. J. O. Aspects of jamming in two-dimensional athermal frictionless systems. *Soft Matter* **10**, 2932–2944 (2014).

57. Boromand, A., Signoriello, A., Lowensohn, J., Orellana, C. S., Weeks, E. R., Ye, F., Shattuck, M. D. & O'Hern, C. S. The role of deformability in determining the structural and mechanical properties of bubbles and emulsions. *Soft Matter* **15**, 5854–5865 (2019).

58. O'Hern, C. S., Silbert, L. E., Liu, A. J. & Nagel, S. R. Jamming at zero temperature and zero applied stress: The epitome of disorder. *Phys. Rev. E* **68**, 011306 (2003).

59. Katgert, G. & van Hecke, M. Jamming and geometry of two-dimensional foams. *Europhys. Lett.* **92**, 34002 (2010).

60. van Hecke, M. Jamming of soft particles: geometry, mechanics, scaling and isostaticity. *J. Phys.: Condens. Matter* **22**, 033101 (2010).

61. Sollich, P., Lequeux, F., Hébraud, P. & Cates, M. E. Rheology of soft glassy materials. *Phys. Rev. Lett.* **78**, 2020–2023 (1997).

62. Antipova, C. G., Krupnin, A. E., Zakirov, A. R., Pobezhimov, V. V., Romanenko, D. A., Stolyarova, D. Y., Chvalun, S. N., Grigoriev, T. E. A Comprehensive Mechanical Testing of Polyacrylamide Hydrogels: The Impact of Crosslink Density. *Polymers* **17**(6), 737 (2025).

63. Gong, J. P., Katsuyama, Y., Kurokawa, T. & Osada, Y. Double-network hydrogels with extremely high mechanical strength. *Adv. Mater.* **15**, 1155–1158 (2003).

Funding

This work was supported by the Dirección General de Asuntos del Personal Académico (DGAPA), Universidad Nacional Autónoma de México (UNAM), through grant PAPIIT IN115124. The authors also acknowledge financial support from the Sistema Nacional de Investigadoras e Investigadores (SNII) of the Secretaría de Ciencia, Humanidades, Tecnología e Innovación (Secihti), Mexico, including the stipends and Postdoctoral Fellowships awarded to C.T.-I. (CVU: 425089) and F.L.G. (CVU: 607354).

Author contributions statement

F.L.G. conceived the system, performed experiments, analyzed results, drafted and revised the manuscript and ensured its integrity. C.T.-I. performed Fourier Analysis, reviewed the manuscript and ensured its integrity. R.F. analyzed results, reviewed the manuscript and ensured its integrity. All authors approved the final version.

Competing interests

The authors declare no competing interests.

Data availability

The datasets used and/or analyzed during the current study are available from the corresponding author (F.L.G.) upon reasonable request.

Additional information

Correspondence and requests for materials should be addressed to F.L.G.